PHYSICAL REVIEW D

PARTICLES AND FIELDS

THIRD SERIES, VOL. 1, NO. 3 1 FEBRUARY 1970

$\pi^- p$ Elastic Scattering between 1.7 and 2.5 GeV/c*

ROGER E. HILL,† NORMAN E. BOOTH,‡ AND ROBERT J. ESTERLING§
Enrico Fermi Institute, The University of Chicago, Chicago, Illinois 60637

AND

SHIGEKI SUWA‖ AND AKIHIKO YOKOSAWA
Argonne National Laboratory, Argonne, Illinois 60440

(Received 12 September 1969)

The polarization and the differential cross section in $\pi^- p$ elastic scattering have been measured at incident pion laboratory momenta of 1.70, 1.88, 2.07, 2.27, and 2.50 GeV/c. The experiment was carried out at the Argonne zero-gradient synchrotron with a polarized proton target. Details of the apparatus and data analysis are presented here together with the final results. A partial-wave analysis of the data has verified the $J^P = 7/2^+$ assignment for the $\Delta(1950)$ and established a $J^P = 7/2^-$ assignment for the $N(2190)$. It does not support a $J^P = 11/2^+$ assignment for the $\Delta(2460)$, nor does it give support for some of the possible resonances found in the CERN phase-shift analysis. Apart from the resonance behavior, the partial-wave analysis reveals several new features. We find a striking correlation among the various partial-wave amplitudes at the highest energy, which is different for $J = l + \frac{1}{2}$ and $J = l - \frac{1}{2}$. In addition, several fixed-$(-t)$ features of high-energy scattering emerge in the energy region of this analysis.

I. INTRODUCTION

PREVIOUS measurements of $\pi^- p$ elastic scattering near 2 GeV/c showed a 2-mb peak in the $\pi^- p$ total cross section,[1] and a prominent second maximum in the differential cross section[2] near $\cos\theta_\pi(\text{c.m.}) = 0.2$. These features indicated that further study in this energy region should be particularly interesting; hence we measured the differential cross section (DCS) and polarization (P) at five momenta spanning the peak in the total cross section. These momenta are listed in Table I along with useful kinematic quantities. Some of our preliminary results have been published previously.[3,4] Our final DCS and P values are given in Tables II–VII and Fig. 5.[5]

Section II describes the apparatus and experimental details; Sec. III describes how we proceeded from our raw data to the final polarizations and cross sections;

TABLE I. Kinematical parameters.

	Beam momentum[a] (GeV/c)	Momentum bite (GeV/c)	Kinetic energy (GeV)	c.m. momentum (GeV/c)	$\bar{\lambda}^2$ (mb)	Total c.m. energy (GeV)
$\pi^- p$	1.700	±0.029	1.566	0.788	0.628	2.025
	1.879	±0.032	1.745	0.837	0.556	2.106
	2.070	±0.035	1.935	0.887	0.495	2.189
	2.266	±0.040	2.131	0.936	0.444	2.272
	2.500	±0.043	2.364	0.991	0.396	2.366
$\pi^+ p$[b]	0.998	±0.017	0.868	0.560	1.239	1.671
pp[c]	0.993	±0.017	0.428	0.448	1.941	2.079

[a] This is the beam momentum at the target center. The 2.08 GeV/c of Ref. 1 refers to the incident beam momentum which, because of energy loss in the target, differs by 14 MeV/c.
[b] For $\pi^+ p$ results see Table VII.
[c] Calibration of target polarization.

---

* Work supported by the U. S. Atomic Energy Commission, the National Science Foundation, and the U. S. Office of Naval Research, under Contract No. Nonr 2121(25).

† Present address: Rutherford Laboratory, Chilton, Didcot, Berkshire, England.

‡ Also of the Physics Department.

§ Present address: Department of Physics, Rutgers, The State University, New Brunswick, N. J. 08903.

‖ Present address: Institute for Nuclear Study, Tokyo University, Tanashi, Tokyo, Japan.

[1] A. N. Diddens, E. W. Jenkins, T. F. Kycia, and K. F. Riley, Phys. Rev. Letters **10**, 262 (1963); A. A. Carter, K. F. Riley, R. J. Tapper, D. V. Bugg, R. S. Gilmore, K. M. Knight, D. C. Slater, G. H. Stafford, E. J. N. Wilson, J. D. Davies, J. D. Dowell, P. M. Hattersley, R. J. Homer, and A. W. O'Dell, Phys. Rev. **168**, 1457 (1968).

[2] D. E. Damouth, L. W. Jones, and M. L. Perl, Phys. Rev. Letters **11**, 287 (1963).

[3] S. Suwa, A. Yokosawa, N. E. Booth, R. J. Esterling, and R. E. Hill, Phys. Rev. Letters **15**, 560 (1965).

[4] A. Yokosawa, S. Suwa, R. E. Hill, R. J. Esterling, and N. E. Booth, Phys. Rev. Letters **16**, 714 (1966).

[5] These are the same values given in the Fermi Institute Report No. 66-29 (unpublished).

Sec. IV gives our results; and Sec. V presents our analysis of the data.

Other measurements of the DCS[6–12] and polarization[13–15] in πp elastic scattering near this energy range have been made concurrently with and subsequent to the completion of this work. Charge-exchange cross sections have also been measured at these energies.[16]

II. DESCRIPTION OF EXPERIMENT

A. General Technique

Figure 1 is a schematic diagram of the apparatus. The incoming pions were counted by a beam telescope and bent downward by the horizontal field of the polarizing magnet. Scatterings were detected in the vertical plane with the target polarization perpendicular to the scattering plane. Only 3% of the nucleons in the target crystals $La_2Mg_3(NO_3)_{12}\cdot 24H_2O$ are hydrogen nuclei and it is these protons which were polarized. Elastic $\pi^- p$ scattering events were separated from other events (inelastic $\pi^- p$ scattering and reactions involving complex nuclei of the target material) by means of the angular correlation between the scattered pion and the recoil proton. Each counter in the A bank of Fig. 1 defines a pion scattering angle. For each A counter, the distribution of coincidences with counters in the B bank is measured. Then, at the conjugate position in the B bank corresponding to elastic $\pi^- p$ scattering, a peak should appear. Scatterings from protons bound in complex nuclei will have a much broadened angular correlation because of the Fermi momentum of the target protons. The correlation of inelastic events will be even less. Moreover, if any third particle is detected, the event cannot be an elastic scattering. Thus we put in anticoincidence counters to cover regions of space other than the A or B banks. The anticoincidence requirement together with a coincidence among any one signal from the A bank, any one from the B bank, and the beam telescope served as a trigger which indicated the possible occurrence of a good event. This trigger allowed the signals from the A and B banks to pass into an encoder which directed the event into a particular memory location of a 32×32 multiscaler. After a run, we examined the resulting distributions and determined the number of events in the elastic peak. By comparing the number of elastic events obtained with positive target polarization (N_+) with the number obtained with negative target polarization (N_-), we obtain the polarization in πp scattering as[17]

$$P=\frac{1}{P_T}\left(\frac{N_+-N_-}{N_++N_-}\right), \qquad (1)$$

where P_T is the magnitude of the target polarization.

B. Polarized Proton Target

The polarized proton target is similar to others already described[18–20] and uses the "solid effect" developed by Abragam[21] and by Jeffries.[19,22] A high degree of nuclear polarization is achieved by inducing "forbidden" transitions which simultaneously flip the nuclear and electron spins in a paramagnetically dilute crystal. Chamberlain *et al.*[23] and Schultz[18] were the first to demonstrate the feasibility of such a target for pion-proton scattering measurements.

Our target consisted of six single crystals of $[La_2Mg_3(NO_3)_{12}\cdot 24H_2O]$ LMN doped with about 1.5% natural Nd. The crystals were cut, stacked, and tied together with Teflon string to give a rectangular-shaped scatterer 19 mm vertical×29 mm horizontal×38 mm long. The crystals were immersed in liquid helium at 1.2°K and were located in a multimode microwave cavity at the center of an 18.6-kG magnetic field. To reach the crystals, the beam had to traverse 0.15 mm of the silver-plated bronze microwave cavity, 0.30 mm of stainless-steel Dewar, 0.25 mm of aluminum radiation shield, 0.15 mm of aluminum outer vacuum jacket, and about 1 cm of liquid helium.

---

[6] C. T. Coffin, N. Dikmen, L. Ettlinger, D. Meyer, A. Saulys, K. Terwilliger, and D. Williams, Phys. Rev. **159**, 1169 (1967).

[7] W. Busza, B. G. Duff, D. A. Garbutt, F. F. Heymann, C. C. Nimmon, K. M. Potter, T. P. Swetman, E. H. Bellamy, T. F. Buckley, P. V. March, R. W. Dobinson, J. A. Strong, and R. N. F. Walker, Phys. Rev. **180**, 1339 (1969).

[8] A. S. Carroll, J. Fischer, A. Lundby, R. H. Phillips, C. L. Wang, F. Lobkowicz, A. C. Melissinos, Y. Nagashima, and S. Tewksbury, Phys. Rev. Letters **20**, 607 (1968).

[9] J. P. Chandler, R. R. Crittenden, K. F. Galloway, R. M. Heinz, H. A. Neal, K. A. Potocki, W. F. Prickett, and R. A. Sidwell, Phys. Rev. Letters **23**, 186 (1969).

[10] D. D. Allen, G. P. Fisher, G. Godden, J. B. Kopelman, L. Marshall Libby, and R. Sears, Nuovo Cimento **53A**, 701 (1968).

[11] B. G. Reynolds, J. D. Kimel, J. R. Albright, R. H. Bradley, E. B. Brucker, W. C. Harrison, B. C. Harms, J. E. Lannutti, W. H. Sims, and R. P. Wieckowicz, Phys. Rev. **173**, 1403 (1968).

[12] S. W. Kormanyos, A. D. Krisch, J. R. O'Fallon, K. Ruddick, and L. G. Ratner, Phys. Rev. **164**, 1661 (1967).

[13] P. J. Duke, D. P. Jones, M. A. R. Kemp, P. G. Murphy, J. J. Thresher, H. H. Atkinson, C. R. Cox, and K. S. Heard, Phys. Rev. **166**, 1448 (1968).

[14] O. Chamberlain, M. J. Hansroul, C. H. Johnson, P. D. Grannis, L. E. Holloway, L. Valentin, P. R. Robrish, and H. M. Steiner, Phys. Rev. Letters **17**, 975 (1966); M. Hansroul, University of California Lawrence Radiation Laboratory Report No. UCRL-17263, 1967 (unpublished).

[15] R. J. Esterling, N. E. Booth, G. Conforto, J. Parry, J. Scheid, D. Sherden, and A. Yokosawa, Phys. Rev. Letters **21**, 1410 (1968).

[16] A. S. Carroll, I. F. Corbett, C. J. S. Damerell, N. Middlemas, D. Newton, A. B. Clegg, and W. S. C. Williams, Phys. Rev. **177**, 2047 (1969).

[17] This is a simplified formula. See Sec. III A.

[18] C. H. Schultz, University of California Lawrence Radiation Laboratory Report No. UCRL-11149, 1964 (unpublished).

[19] C. D. Jeffries, *Dynamic Nuclear Orientation* (Wiley-Interscience, Inc., New York, 1963).

[20] G. Shapiro, Progr. Nucl. Tech. Instr. **1**, 173 (1964). For a recent survey of targets see *Proceedings of the Conference on Polarized Targets and Ion Sources, Saclay, France, 1966* (La Documentation Française, Paris, 1967).

[21] A. Abragam and W. J. Proctor, Compt. Rend. **246**, 2253 (1958); A. Abragam and M. Borghini, *ibid.* **248**, 1803 (1959).

[22] T. J. Schmugge and C. D. Jeffries, Phys. Rev. Letters **9**, 268 (1962).

[23] O. Chamberlain, C. D. Jeffries, C. H. Schultz, G. Shapiro, and L. Van Rossum, Phys. Rev. Letters **7**, 293 (1963).

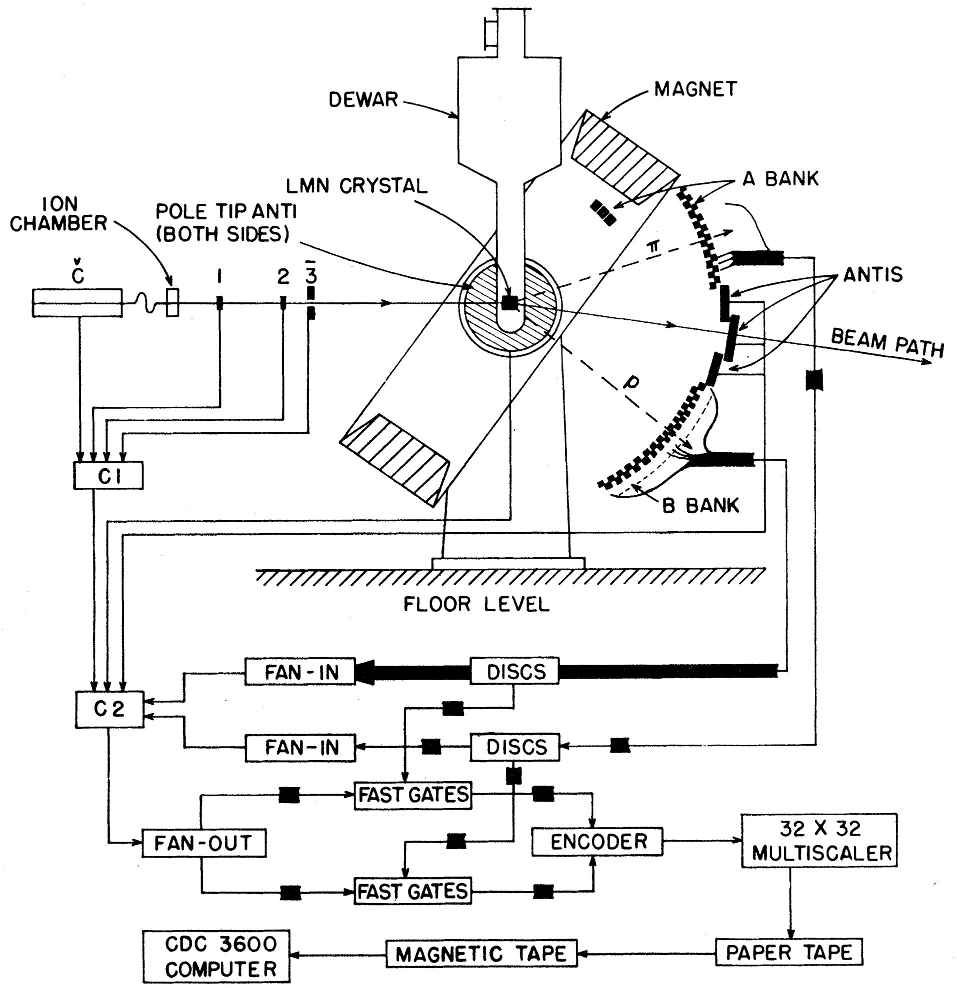

Fig. 1. Schematic view of the apparatus. Č is the Čerenkov counter: $C1$ and $C2$ are coincidence circuits. The heavy lines indicate a cable for each counter of the A or B bank.

The "forbidden" transition frequency is supplied by a Carcinotron backward wave oscillator which operates at ~70 GHz. To prevent the Carcinotron from drifting off the transition frequency we used a phase-sensitive feedback detector.[24] The direction of proton polarization can be reversed by changing the microwave frequency by 0.2% to saturate the transition with the reverse nuclear polarization. We must stress that this small frequency change is the only change we made in going from one sign of target polarization to the other. This method of reversing the target polarization eliminates many systematic errors that otherwise might be present in the asymmetry if, for example, we had to change the magnetic field or move the counters.

The magnitude of the target polarization was measured with a nuclear-magnetic-resonance (NMR) detection system. Depending in which direction the protons are polarized, the proton spins at their resonance frequency (79.5 MHz for 18.6 kG) absorb energy from or release energy to the radio-frequency (rf) field provided by an rf generator. The amount of energy exchanged is proportional to the magnitude of the proton polarization. A Q-meter-type detector was used to detect the resonance of the crystals. The rf voltage V was amplified, rectified, monitored on a chart recorder, digitized using a voltage-to-frequency converter, and punched onto paper tape for later computer calculation of the polarization. A slight modulation of the magnetic field at 100 cps and a lock-in amplifier were used to obtain and record a signal proportional to the derivative of V with respect to the rf frequency ν. Because the local magnetic field varies from place to place in the crystal, the proton resonance is not just a single line but consists of several levels, and we must sweep over all the resonance lines in order to get a signal representative of all the protons in the crystal. The target polarization was then calculated from the

---

[24] Developed by A. Moretti and K. Bourkland, Argonne National Laboratory.

formula[25]

$$P_T=k\int[V(\nu)-V_0]/V(\nu)d\nu\,, \tag{2}$$

where V_0 is the rf voltage at an off-resonance point.

The proportionality constant k was determined by integrating the $dV/d\nu$ signal measured with the target at thermal equilibrium (i.e., microwave power off). At thermal equilibrium the proton polarization may be readily calculated from the Boltzmann factor.

During a run the V and $dV/d\nu$ signals were recorded every 15 min. An average P_T for each run was obtained by weighting each NMR signal by the number of pions incident between adjacent signals. Target polarizations were typically between 0.5 and 0.6. Values of P_T obtained from Eq. (2) were considered to be only relative. The normalization of the target polarization is discussed in Sec. III C.

C. Pion Beam

The pion production target was a 10-cm-long piece of Cu placed slightly inside octant 4 of the zero-gradient synchrotron (ZGS). Negative particles produced at 0° were deflected 17° by the magnetic field of the ZGS into a standard beam transport system consisting of six quadrupole magnets and two bending magnets.[26] The beam was focused both at the polarized target and at a point intermediate between the two bending magnets. The solid-angle acceptance of the beam ($\sim 2.4\times10^{-4}$ sr) was determined by the first two quadrupole lenses. A collimator at the intermediate focus determined the momentum acceptance as $\Delta p/p=\pm0.017$. The absolute momenta are known to better than 1%. At the polarized target the beam profile was typically 18 mm vertical (FWHM) and 15 mm horizontal with ±3-mrad-vertical and ±5-mrad-horizontal angular divergence. Profiles were taken periodically with a 3×3-mm scintillator mounted on a movable table. We also had two L-shaped counters mounted on either side of the beam. The ratio of their counting rates served as a sensitive indicator of beam shifts.

The beam was monitored and defined by the counters 1–3 (shown in Fig. 1) in the coincidence circuit $C1$. Counter 3 is a large counter with a 16-mm-vertical×25-mm-horizontal hole in the center through which the beam passed. Since counters 1 and 2 were slightly larger than this hole, counter 3 gave the final definition of the beam size. An ion chamber was also used to monitor the beam; it agreed well with the counters but was less accurate because of its insensitivity to beam size and position. The average beam intensity was 1.5×10^5 pions/pulse with typical beam spill time of 250 msec.

Accidentals in the beam telescope (two beam particles coming within the resolution of our coincidence circuit) were measured by putting two signals from the beam telescope in coincidence but with one signal delayed by one synchrotron rf period (≈ 70 nsec). The accidentals were always less than 10% and were typically 3% of the total beam. The measured accidentals were *subtracted* from the scaled number of pions in each run—subtracted because a second beam particle would have a high probability of vetoing a good event were it produced by the first beam particle. (The forward anticoincidence counters and the pole tip counter vetoed $\approx 95\%$ of the $C1$ events; see Sec. II D.)

The target crystals were aligned with the beam to ±1 mm by taking an x ray to determine the crystal location inside the cold Dewar, and by adjusting the magnet height to the impact parameter calculated for each momentum.

The pion beam was contaminated with both electrons and muons. The electrons were electronically removed by a threshold gas Čerenkov counter[27] in anticoincidence with the beam telescope. We have independent evidence from our scattering distributions that the Čerenkov counter was effective in removing these electrons (see Sec. II F).

The muon contamination of the beam was calculated by integrating along the beam path the product of the probability that a pion decays into a muon and the probability that a muon can pass through our beam-defining telescope. This calculation gives muon contaminations ranging from 2.7% at 2.5 GeV/c to 2.0% at 1.7 GeV/c, with an uncertainty of perhaps 0.5%.

D. Counter Configuration

The general layout of the counters is shown in Fig. 1; the beam counters were discussed above. All counters were made of plastic scintillator, either 6 or 12 mm thick. The main A and B banks were constructed so that each counter subtended a polar angle of 1.5° in the lab. The counters were placed alternatively on a 102- and a 107-cm radius from the center of the magnet. The bank was designed such that a particle coming along any radius would see a continuous bank of counters with no overlapping or gaps. Unfortunately, because of the magnetic field, particles did not travel along radii from the center of the magnet; hence, some particles did miss the counters (see Fig. 2). This effect necessitated a correction in the cross sections as discussed in Sec. II D.

The counters were constructed such that the acceptance in azimuthal angle was about ±10° for all polar angles. This ±10° azimuthal acceptance was the only

---

[25] A. Moretti, S. Suwa, and A. Yokosawa, in *Proceedings of the International Conference on Polarization Phenomena of Nucleons, Karlsruhe, 1965*, edited by P. Huber and H. Schopper (W. Rosch and Co., Bern, 1966).

[26] The beam was essentially the same as that described in Refs. 6 and 12 and was originally designed by K. Terwilliger and D. Williams.

[27] Kindly loaned to us by D. Meyer of the University of Michigan.

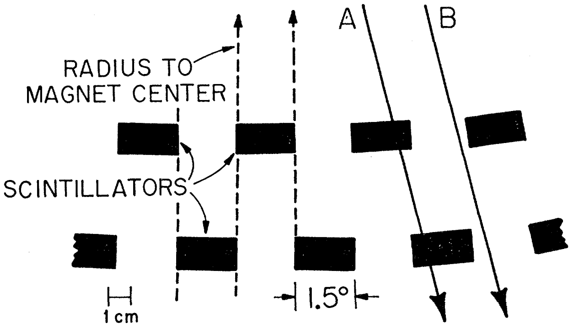

FIG. 2. Cross-sectional view of a segment of the counter banks. Trajectory A represents a particle coming in at an angle to the radius vector and which goes through two adjacent counters; trajectory B represents a similar particle which goes through the gap between two adjacent counters.

coplanarity requirement that we used for most of the runs.

The lower limit in pion c.m. angles which we could measure was determined by the range of recoil protons in the rather thick target crystals. Each bank was positioned so that we would obtain this low c.m. angle and the physical extent of the bank (36° for the A bank, 43.5° for the B bank) determined the upper c.m. angle limit for the bank. The angular position of each counter was measured to 0.1° using a sine-bar arrangement attached to each bank of counters.

In addition to the main banks of counters, we also had "yoke" counters at 43°, 49°, and 55° above the beam line and 103° and 135° below the beam; these counters effectively extended the range of the A and B banks, respectively. The "yoke" counters were situated on a 48-cm radius and were designed to fit inside the magnet yoke.

Each yoke counter covered 3° in polar angle and ±10° in azimuthal angle. The yoke counters acted only as defining counters; the top yoke counters had their conjugate particle coming in the B bank, while the bottom yoke counters had their conjugate particle detected in the A bank. These yoke counters enabled us to obtain some data points in the backward direction in the c.m. system. The main reason why we did not obtain more points was that the low cross section in the backward direction did not allow us to distinguish elastic events from the background.

To reduce background from inelastic processes, we had several anticoincidence counters placed such that they would veto any three or more particle events. Counters placed on the accessible region of the magnet pole faces reduced our background by a factor of 3. A counter placed in the beam after the polarized target reduced the background by an additional 50%, both by vetoing forward inelastic events and by signaling beam particles that did not interact in the target. Additional anticoincidence counters helped us restrict the azimuthal acceptance of the A and B banks.

E. Electronics

The main function of the fast electronic logic was to determine that a possible good event occurred; slow logic[28] then stored that event in a particular memory location of a multiscaler.

Most of the photomultipliers were RCA 6199 tubes, but we used Zener diode stabilized 56AVP photomultipliers on all counters that experienced a high rate. The high voltage on each counter in the A and B banks was set by requiring all the counters to yield 0.1-V output pulse when excited by Co^{60} γ rays. Previous experience with plateauing these counters in the beam showed that this response yielded high counter efficiencies.

A simplified schematic of the electronics is shown in Fig. 1. The delays of all pulses were set by observing the appropriate coincidence rate versus delay setting. The relative delays between counters in A or B banks were adjusted with small cable lengths to account for individual phototube differences. The resolving time of the $C2$ coincidence was made sufficiently wide (15 nsec) to include all time-of-flight differences from one end of the elastic region to the other. Once a $C2$ trigger was obtained, the $C1$ coincidence circuit was gated off until the event had been stored in the multiscaler or rejected by the slow logic. Thus there is no dead-time correction. A $C2$ trigger means that at least one A counter and one B counter had fired in coincidence with an incoming pion with no anticoincidence counter responding at the same time. The $C2$ trigger then allowed any pulses from counters that had fired in the A or B banks to pass a gate into the slow logic.

If more than one counter of either the A or the B bank had fired, the slow logic scaled the event as a "multiple." If a multiple event came from adjacent counters in the B bank, the event was also scaled as an "adjacent" and the fast logic was reset to receive additional events. If the event was not a multiple, the slow logic translated the counter numbers into a memory address code and added one to that memory location. After a run the entire memory of the multiscaler was both printed and punched onto paper tape.

There were several test routines built in to the logic which checked the operation of the system. The most important of these was a light pulser that sequentially pulsed nanosecond light discharges in hydrogen corona lamps optically coupled to each counter of the A and B banks. Inherent in this test were the requirements that all phototubes and electronic circuits were working properly, that all cables were continuous and properly connected to the right counters and gates, that the coincidence timings were correct, and that each A and B combination was stored in the correct multiscaler memory location.

---

[28] Designed and constructed by R. Marquadt and J. Simanton, IEEE Trans. Nucl. Sci. **13**, 174 (1966).

F. Data Collection—Scattering Distributions

Data were usually accumulated in runs of 2–4-h duration after which the scattering data were recorded and the target polarization reversed for the ensuing run. A typical scattering distribution is shown in Fig. 3.[29] It was chosen to illustrate several features: (1) The cross section for these points are among the *lowest* we measured (100 μb/sr); (2) it contains both a narrow pion defining peak and a wide proton defining peak, giving results for two different c.m. angles for the same counters; and (3) it has some residual electron background. This particular defining counter ($A24$) had two peaks in the conjugate (B) bank corresponding to either a proton or a pion passing through counter $A24$. That is, whenever an elastically scattered pion registered in counter $A24$, its conjugate proton came near the angle covered by counter $B9$. Similarly, if an elastically scattered proton came in $A24$, its conjugate pion registered near counter B24. Usually there is some angular region where these peaks overlap and one cannot distinguish a pion from a proton. However, in our case of π^-p scattering, the magnetic field causes complete separation of the peaks for all angles. This is not the case for π^+p scattering, where the overlap is worse than if there were no magnetic field. The proton peak is wider than the pion mostly because the c.m.-to-lab transformation is different for the two particles (the magnetic field also contributes). As can be seen in Fig. 3, the Monte Carlo program adequately accounts for the peak widths (see Sec. III B).

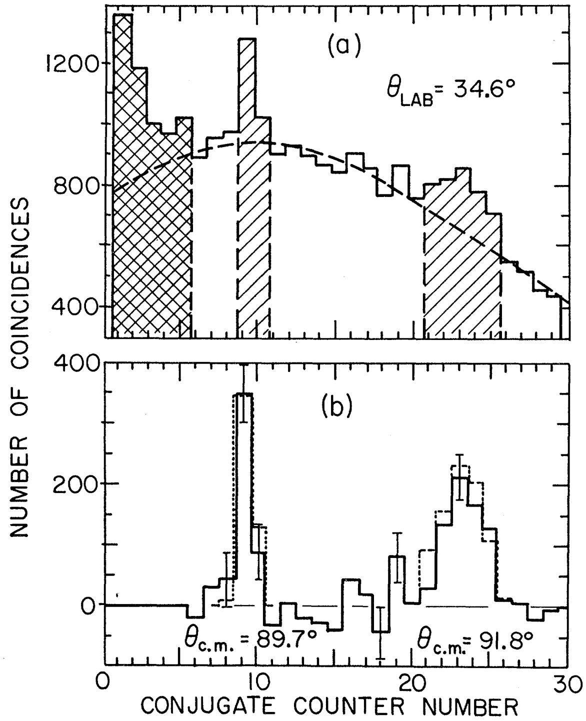

FIG. 3. A typical coincidence distribution (defining counter $A24$ at 2.27 GeV/c for $+P_T$). (a) Raw data showing both an elastic pion defining and proton defining peak. The dashed line is a computer fit to the background, i.e., to the region outside the shaded areas. The cross-hatched area contains background due to beam electrons. Note that the vertical scale starts at 300: The given lab angle is measured from horizontal, not from the beam. (b) The solid lines give the elastic peaks that remain after background subtraction. The dotted lines are Monte Carlo simulations of the same data.

Most of the background comes from quasi-elastic π^-p scatterings from the bound protons in the complex nuclei of the crystal. This background has a Gaussian-like shape. The majority of the inelastic background has been eliminated by the anticoincidence counters. The remaining background at low conjugate counter number (in the forward direction—low pion c.m. angles) is from beam electrons that were not vetoed by the Čerenkov counter (see Sec. II C). They appear in this run because the Čerenkov counter was slightly misaligned. With the Čerenkov counter working properly, all of this exponential tail disappeared. Without the Čerenkov counter and a 10% electron contamination in the beam, the over-all background increased by a factor of 10 and the huge exponential tail made the experiment unfeasible.

III. DATA REDUCTION

A. Data Handling

The first step in reducing the data was the conversion of the punched paper tapes to a magnetic tape that served as a library of all information received from the multiscaler. A computer program then took sorted data from this tape, made a fit to the background for each defining counter, plotted the data and the fit on an oscilloscope, and finally computed the polarization and cross section with their respective errors.

The dashed line in Fig. 3(a) shows a typical computer fit to a background. A least-squares program was used to fit the region outside the shaded regions to a function that was the sum of a Gaussian and a linear term (five parameters). In this particular case the electron background (cross-hatched area) was not fitted. However, in some cases the electron background was fitted by adding an exponential function (two more parameters).[29] The elastic peak region that was not fitted was determined mainly by a Monte Carlo program that predicted the peak's position and width (see Sec. III B). However, some judgment did enter into this determination on the edges of the peaks. For example in Fig. 3, should conjugate counter 8 be included in the pion peak or not? The uncertainty of such judgments was generally included in the statistical uncertainty of each point.

The assumption that one may fit a smooth mathematical background outside the peak region and then

---

[29] Another one of our distributions is given in Fig. 2 of Ref. 3. It shows a computer plot of a fit to the background including an exponential electron tail.

interpolate under the peaks was tested extensively at the Chicago cyclotron by comparing background fits to p-p scattering data from a LMN target with data from a dummy target. The dummy target was constructed to have about the same nuclear composition as the LMN target but without any hydrogen nuclei present. In all tests the shape of the distributions from the dummy target agreed well with the background fits to the LMN target. No runs were made at the ZGS with a dummy target.

If we let C equal the total number of counts in the peak regions (the shaded areas of Fig. 3), B equal the number of (fitted) background counts under the peak, π equal the scaled number of incident pions, ρ equal target proton density, t equal target thickness, P_T equal the magnitude of the beam weighted average target polarization, Ω equal the c.m. solid angle of each counter, and the + and − superscripts stand for positive and negative target polarizations, respectively, then the average background rate is $b=\frac{1}{2}(B^+/\pi^+ + B^-/\pi^-)$, the number of counts under each peak is $n^\pm = C^\pm/\pi^\pm - b$, and the DCS is

$$\frac{d\sigma}{d\Omega}=\frac{n^-P_T^+ + n^+P_T^-}{\rho\Omega t(P_T^+ + P_T^-)}. \tag{3}$$

The polarization is given by

$$P=\frac{C^+/\pi^+ - C^-/\pi^-}{n^-P_T^+ + n^+P_T^-} \tag{4}$$

and

$$P\frac{d\sigma}{d\Omega}=\frac{C^+/\pi^+ - C^-/\pi^-}{\rho\Omega t(P_T^+ + P_T^-)}. \tag{5}$$

Note that the assumption that b is the same for both target polarizations causes b to drop out of Eq. (5) and to affect P only slightly. Since most of the background comes from the unpolarized nucleons of the complex nuclei in the target, this assumption should be good, and in practice b^+ and b^- always agreed within their statistical uncertainty. These formulas properly account for differences in P_T^+ and P_T^-, since, in general, they were not equal. The sign of P is established by the convention that P_T is positive if the proton spins are parallel to $\mathbf{k}_i \times \mathbf{k}_f$, where $\mathbf{k}_i$ and $\mathbf{k}_f$ are the momentum vectors of the incident and the outgoing pions. The determination of t and Ω is discussed in Sec. III B, the uncertainty in P_T in Sec. III C, and the DCS normalization in Sec. III D.

The most ambiguous part of the data reduction is to decide what error to assign to b. In general, we took $\delta b=\frac{1}{2}[(B^+)^{1/2}/\pi^+ + (B^-)^{1/2}/\pi^-]$, but this error is too large for narrow peaks because one has neglected the information contained in fitting the entire spectrum. It is too small for wide peaks because it neglects systematic uncertainties in interpolating under the peaks. In the final analysis each distribution was examined carefully to be sure that the computer fit was reasonable and that possible variations of the fit were included in the background error.

B. Monte Carlo Program

The three most important numbers computed by the Monte Carlo program were the solid angle, scattering angle, and angular resolution of each defining counter in the c.m. system. However, it also computed the effective target thickness, the conjugate particle lab angle, and the peak width for each counter. These items are nontrivial to calculate mostly because the magnetic field of the polarized target causes the particle orbits to curve. Even so, it would not be necessary to have a Monte Carlo program except that multiple scattering and varying amounts of energy loss in combination with the magnetic field make it difficult to compute the solid angle of a particular counter.

Basically, the Monte Carlo program was designed to follow the incident and scattered particles, to calculate quantities that are determined by the geometry or kinematics, and to randomly choose variables which depend on chance. Items taken into account by the program include the momentum and spatial spread and the angular divergence of the beam, the nonuniform magnetic field, multiple scattering and energy loss in the cryostat components, the helium, and the target crystal. Nuclear absorption was not included and is discussed further in Sec. III D.

The effective LMN target thickness was taken to be the average distance traveled in the crystal by a Monte Carlo beam particle. This differs from the measured target thickness for the following reasons: (1) The magnetic field bends the beam by about 4° before it reaches the LMN; (2) the path in the LMN is a slightly curved arc; and (3) the spatial spread and angular divergence of the beam causes some particles to miss part or all of the LMN. The net result is that the measured target thickness is too large by (5±3)%. The error arises mostly because of the uneven sides of the LMN crystals and because of the uncertain angular divergence of the beam.

C. Target Polarization Calibration

Relative target polarizations were continuously measured with the NMR system described in Sec. II B. Because the ratio of enhanced to thermal-equilibrium polarization is 10^3 and because the beam may not sample the target in the same manner as the NMR-system, the absolute target polarization remains uncertain. In order to check the NMR polarization calculation, we measured the asymmetry in p-p elastic scattering at 423 MeV and compared our results with previous measurements that used polarized proton beams.

The experimental arrangement for the p-p scattering was basically the same as in Fig. 1. Although the

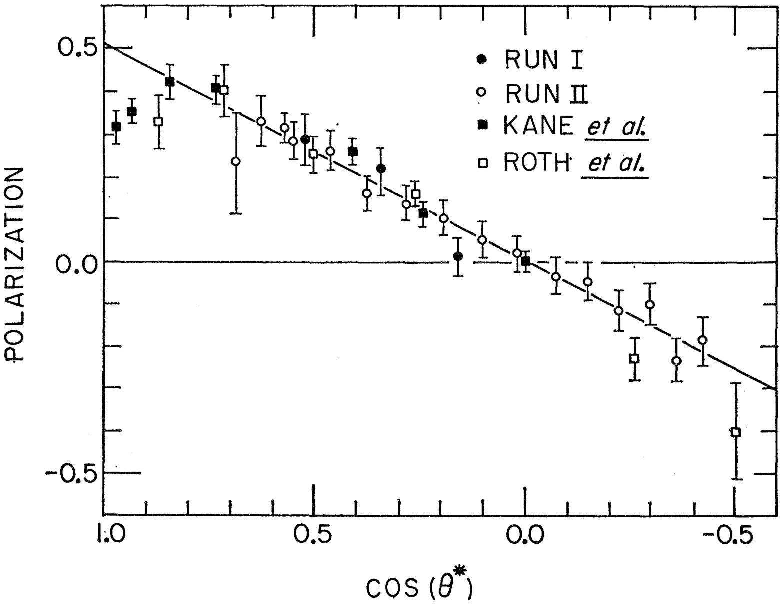

FIG. 4. Polarization in p-p elastic scattering at 423 MeV. Our data are the circular points; the squares are the data of Kane *et al.* (Ref. 31) and of Roth *et al.* (Ref. 30).

incident proton beam may have had a net polarization in the vertical direction, the beam was effectively unpolarized since the scattering took place in the vertical plane. Two separate p-p scattering runs were made. In the first run the beam was bent up and the asymmetry was measured at three scattering angles; in a second run, made three months later, the beam was bent down and measurements were made at many more angles and over a wider angular region. The Čerenkov counter was used to discriminate between π^+ and protons and, in fact, during the first run a pulse from the Čerenkov counter was used to route events to different locations in the multiscaler depending upon whether a π^+ or a proton was incident. Thus, we were able to accumulate π^+ and proton data simultaneously (see Table VII).

Our results for p-p polarization are shown in Fig. 4. Also plotted in the same figure are the data of Roth *et al.*[30] at 430 MeV and the data of Kane *et al.*[31] at 415 MeV. At least-squares fit of the straight line $A\cos(\theta^*)$ to our data gives $A=0.52\pm0.04$. A similar fit to the other data for $\cos\theta<0.75$ gives $A=0.566\pm0.024$. Thus, P_T(from p-p scattering) $=(0.92\pm0.07)P_T$(NMR).

In accordance with this calibration, all our π^-p polarization data computed with P_T(NMR) have been divided by 0.92. In addition to the statistical error on the above calibration, there are two sources of systematic error which contribute to the uncertainty in the *absolute* target polarization: (1) The polarization data of Roth *et al.* and Kane *et al.* have a normalization error of $\pm10\%$, due to uncertainty in beam polarization; and (2) P_T(NMR) is obtained by comparing the enhanced NMR signals with the thermal-equilibrium (TE) NMR signals. The TE signals have been found to fluctuate from day to day by about $\pm8\%$. Combining these systematic effects with the statistical error in the calibration, we obtain an over-all uncertainty of $\pm15\%$ in the absolute normalization of P_T. This uncertainty has not been included in any of the quoted errors, but it must be recognized in any analysis of this work.

D. Cross-Section Normalization Corrections

Despite the complications of a magnetic field and a dense target consisting mainly of complex nuclei, we made a serious attempt to absolutely normalize our DCS data. Most of the factors that affect a measurement of an absolute DCS have been mentioned previously—beam monitoring, muon and electron contamination, accidentals, and target alignment in Sec. II C, the solid-angle computation and the effective target thickness in Sec. III B. A discussion of the "adjacents" and the nuclear-absorption corrections follows.

Because the counters were constructed on two different radii from the target center, some particles went through two adjacent counters (adjacents) and others went through the gaps between the counters (gaps) as is shown in Fig. 2. Adjacents were scaled but otherwise rejected by the slow electronic logic. Gaps were not recorded at all, since the event did not satisfy the fast-logic trigger requirement. Because these are otherwise good events, the DCS must be raised by about 8% to correct for the particles that are lost.

In principle, the Monte Carlo program could calculate this adjacents correction. However, possible small ($\frac{1}{2}$-mm) misalignments between counters increases the

---

[30] R. Roth, E. Engels, S. C. Wright, P. Kloeppel, R. Handler, and L. G. Pondrom, Phys. Rev. **140**, B1533 (1965).

[31] J. A. Kane, R. A. Stallwood, R. B. Sutton, T. H. Fields, and J. G. Fox, Phys. Rev. **95**, 1694 (1954).

correction. Furthermore, the scaled adjacents rate need not agree with the computed rate because elastically scattered particles will, in general, have a smaller angle of incidence upon each counter bank than inelastic or quasi-elastic events. Because these two factors are so uncertain, we estimate that the adjacents correction could be in error by as much as a factor of 2 and thus gives the largest uncertainty in obtaining an absolute DCS.

Because the target crystal consists mostly of heavy elements, there is a considerable probability that any given particle will interact with some target nucleus. If either the beam particle or either of the secondary particles from a valid event scatters in the LMN crystal or in the cryostat, that event is lost because the scattering destroys the angular correlation of the secondary particles. Thus we must correct the DCS for nuclear scattering. The nuclear absorption of a secondary particle was computed by calculating its path length in matter for each c.m. scattering angle, using the appropriate cross section as a function of the particle energy, and averaging over the spatial interaction distribution in the target. The over-all correction for nuclear absorption was (14±3)% and was almost independent of c.m. scattering angle. The error on this correction arises mostly from the uncertainty in the heavy-element cross sections.

When all the corrections mentioned above were applied to our DCS data, we compared our p-p DCS at 423 MeV with published data near this energy.[32] The ratio of the average of several previous experiments to our average p-p DCS of 3.359±0.036 mb is 1.082 ±0.016. Also, we compared out π^-p DCS measurements at 2.5 GeV/c with those of Coffin *et al.*[6] at the same momentum in the angular region where the two overlap. The ratio of their data to ours is 1.066±0.030. The agreement of these two ratios is good, implying that our DCS measurements may be low by 7–8%. This difference is within the systematic uncertainties of our DCS corrections, and could be due entirely to the adjacents correction described above. If we add in quadrature all our estimated systematic errors, we obtain a +12, −9% normalization uncertainty. Within this uncertainty, our cross sections compare well with other data.

IV. DCS AND POLARIZATION RESULTS

The π^-p DCS and polarization results are given in Tables II–VI, and are shown graphically in Fig. 5. Three π^+p points, obtained during the first p-p calibration run, are given in Table VII. The DCS values in the tables are our corrected values; the quoted errors are 1 statistical standard deviation.

Because of the systematic errors in our DCS corrections, *in the data analysis* and in Fig. 5 (but not in the tables) we multiplied our DCS values by 1.066 to be consistent with the Michigan data[6] at 2.50 GeV/c. Thus we effectively normalize all our DCS data to the Michigan data at 2.50 GeV/c. Note that the Michigan group believes that their absolute normalization is good to ±5%.

At 1.70, 1.88, and 2.27 GeV/c our DCS data in Fig. 5 are supplemented at larger angles by preliminary data

TABLE II. Experimental results at 1.70 GeV/c.

$\cos\theta_\pi$ (c.m.)	$\Delta(\cos\theta)$	$-t$ [(GeV/c)^2]	$d\sigma/d\Omega$ (mb/sr)	P	$P\,d\sigma/d\Omega$ (mb/sr)
0.856	0.012	0.179		−0.192±0.050	−0.62 ±0.16
0.827	0.013	0.215	2.46 ±0.20	−0.205±0.041	−0.51 ±0.10
0.795	0.015	0.255	1.831±0.088	−0.172±0.048	−0.315±0.088
0.759	0.015	0.299	1.432±0.063	−0.145±0.050	−0.207±0.072
0.724	0.016	0.343	1.078±0.046	−0.087±0.057	−0.094±0.061
0.686	0.017	0.390	0.681±0.039	0.089±0.072	0.061±0.049
0.647	0.017	0.438	0.531±0.030	0.233±0.089	0.123±0.047
0.606	0.017	0.489	0.299±0.022	0.28 ±0.12	0.084±0.036
0.565	0.018	0.540	0.246±0.021	0.52 ±0.15	0.129±0.037
0.524	0.019	0.591	0.186±0.024	0.60 ±0.22	0.112±0.041
0.480	0.019	0.646	0.123±0.020	0.53 ±0.28	0.065±0.035
0.437	0.020	0.699	0.156±0.021	0.50 ±0.23	0.079±0.037
0.375	0.044	0.776	0.178±0.016	0.24 ±0.13	0.043±0.023
0.306	0.020	0.862	0.246±0.020	0.00 ±0.21	−0.001±0.052
0.262	0.020	0.917	0.202±0.024	−0.11 ±0.19	−0.022±0.039
0.220	0.020	0.969	0.254±0.025	−0.15 ±0.16	−0.038±0.042
0.209	0.047	0.982		−0.11 ±0.12	−0.027±0.029
0.177	0.020	1.022	0.216±0.021	−0.26 ±0.17	−0.057±0.036
0.135	0.020	1.074	0.238±0.022	−0.03 ±0.15	−0.007±0.037
0.053	0.020	1.176	0.280±0.026	−0.09 ±0.15	−0.026±0.042
0.013	0.020	1.226	0.218±0.024	−0.45 ±0.19	−0.098±0.042
−0.054	0.012	1.309	0.191±0.031	−0.49 ±0.23	−0.094±0.044
−0.122	0.033	1.393	0.181±0.033	−0.66 ±0.23	−0.120±0.041
−0.256	0.032	1.560	0.230±0.049	−1.15 ±0.26	−0.265±0.060
−0.372	0.028	1.704	0.309±0.049	−0.65 ±0.22	−0.202±0.067
−0.635	0.013	2.030		−0.21 ±0.27	−0.026±0.033

---

[32] W. N. Hess, Rev. Mod. Phys. **30**, 368 (1958).

TABLE III. Experimental results at 1.88 GeV/c.

$\cos\theta_\pi$ (c.m.)	$\Delta(\cos\theta)$	$-t$ [$(\mathrm{GeV}/c)^2$]	$d\sigma/d\Omega$ (mb/sr)	P	$P\,d\sigma/d\Omega$ (mb/sr)
0.865	0.012	0.189		−0.282±0.063	−0.79 ±0.18
0.833	0.013	0.234	2.03 ±0.13	−0.293±0.042	−0.595±0.085
0.800	0.014	0.280	1.507±0.096	−0.194±0.049	−0.292±0.074
0.765	0.015	0.329	1.044±0.045	−0.200±0.056	−0.209±0.058
0.728	0.016	0.381	0.751±0.035	−0.043±0.068	−0.032±0.051
0.688	0.017	0.437	0.534±0.028	−0.018±0.084	−0.010±0.045
0.648	0.018	0.493	0.335±0.021	0.20 ±0.11	0.069±0.037
0.606	0.018	0.552	0.242±0.019	0.33 ±0.15	0.080±0.035
0.541	0.041	0.643	0.137±0.012	0.37 ±0.14	0.051±0.019
0.475	0.019	0.736	0.118±0.018	−0.09 ±0.25	−0.011±0.029
0.430	0.019	0.799	0.160±0.016	−0.27 ±0.17	−0.044±0.028
0.385	0.020	0.862	0.137±0.016	−0.36 ±0.20	−0.049±0.028
0.340	0.020	0.925	0.243±0.025	−0.22 ±0.16	−0.053±0.039
0.295	0.020	0.988	0.265±0.024	−0.24 ±0.14	−0.064±0.037
0.229	0.042	1.080	0.344±0.019	−0.253±0.085	−0.087±0.029
0.163	0.020	1.173	0.319±0.026	−0.16 ±0.13	−0.052±0.042
0.120	0.020	1.233	0.308±0.030	−0.13 ±0.14	−0.040±0.042
0.078	0.020	1.292	0.258±0.021	−0.18 ±0.15	−0.047±0.038
0.037	0.019	1.349	0.246±0.026	−0.22 ±0.17	−0.053±0.042
−0.020	0.035	1.429	0.218±0.019	−0.37 ±0.12	−0.081±0.026
−0.091	0.030	1.529	0.187±0.019	−0.55 ±0.17	−0.103±0.032
−0.146	0.033	1.606	0.178±0.017	−0.42 ±0.19	−0.075±0.034
−0.280	0.029	1.793	0.228±0.023	−0.58 ±0.19	−0.132±0.043
−0.397	0.027	1.957	0.242±0.032	−0.60 ±0.24	−0.145±0.058
−0.661	0.013	2.327		−1.60 ±1.36	−0.060±0.051

communicated to us by the UC/WC collaboration.[7] Normalization factors of 1.05±0.07, 1.07±0.06, and 0.97±0.06 have been applied to their preliminary data at the three respective momenta. These normalization factors were obtained by a point-to-point comparison between their data and our renormalized data in the angular region where the two experiments overlap.

At 2.07 GeV/c we have included some data[2] obtained in a spark-chamber experiment at 2.01 GeV/c. Because of the slight difference in the two momenta, we used the four-momentum transfer rather than the scattering angle as the common variable. The resulting DCS values from Ref. 2 were multiplied by 1.22±0.04 to renormalize them, again by means of a point-to-point comparison.

At 2.50 GeV/c our DCS data are supplemented by the Michigan results.[6]

At all momenta we included a DCS measurement at 180° by Kormanyos *et al.*[12] and a point at 0° calculated from the total cross section and the ratio of real to

TABLE IV. Experimental results at 2.07 GeV/c.

$\cos\theta_\pi$ (c.m.)	$\Delta(\cos\theta)$	$-t$ [$(\mathrm{GeV}/c)^2$]	$d\sigma/d\Omega$ (mb/sr)	P	$P\,d\sigma/d\Omega$ (mb/sr)
0.838	0.013	0.255	2.02 ±0.11	−0.119±0.032	−0.242±0.066
0.804	0.014	0.308	1.426±0.056	−0.100±0.040	−0.143±0.058
0.768	0.015	0.365	0.848±0.034	0.011±0.050	0.009±0.042
0.730	0.016	0.425	0.455±0.026	0.070±0.071	0.032±0.032
0.689	0.017	0.489	0.304±0.024	0.345±0.080	0.105±0.024
0.647	0.018	0.555	0.191±0.018	0.49 ±0.13	0.095±0.025
0.604	0.019	0.623	0.096±0.017	0.55 ±0.20	0.053±0.019
0.560	0.019	0.692	0.097±0.014	0.39 ±0.20	0.038±0.019
0.541	0.037	0.722		0.02 ±0.33	0.002±0.032
0.516	0.019	0.762	0.108±0.016	0.15 ±0.19	0.016±0.020
0.470	0.020	0.834	0.121±0.015	−0.37 ±0.17	−0.045±0.020
0.421	0.019	0.911	0.144±0.016	−0.66 ±0.16	−0.095±0.023
0.402	0.044	0.941		−0.41 ±0.14	−0.070±0.024
0.378	0.019	0.979	0.219±0.019	−0.33 ±0.12	−0.072±0.026
0.331	0.020	1.053	0.225±0.021	−0.62 ±0.12	−0.139±0.026
0.284	0.021	1.127	0.301±0.021	−0.23 ±0.10	−0.071±0.030
0.239	0.046	1.197	0.333±0.020	−0.309±0.054	−0.103±0.018
0.193	0.020	1.270	0.359±0.026	−0.139±0.091	−0.050±0.033
0.148	0.020	1.341	0.308±0.020	−0.140±0.090	−0.043±0.028
0.105	0.020	1.408	0.338±0.034	−0.374±0.091	−0.126±0.031
0.061	0.020	1.478	0.305±0.024	−0.33 ±0.10	−0.102±0.031
0.010	0.040	1.558	0.245±0.018	−0.304±0.065	−0.075±0.016
−0.168	0.033	1.838		−0.79 ±0.35	−0.062±0.027
−0.299	0.031	2.044		−0.52 ±0.49	−0.034±0.032
−0.416	0.027	2.228		−0.65 ±0.45	−0.045±0.031

TABLE V. Experimental results at 2.27 GeV/c.

$\cos\theta_\pi$ (c.m.)	$\Delta(\cos\theta)$	$-t$ [(GeV/c)^2]	$d\sigma/d\Omega$ (mb/sr)	P	$P\,d\sigma/d\Omega$ (mb/sr)
0.903	0.010	0.170		−0.071±0.038	−0.25 ±0.14
0.875	0.011	0.219		−0.040±0.025	−0.094±0.058
0.843	0.013	0.275	1.623±0.052	−0.086±0.028	−0.139±0.046
0.809	0.014	0.335	0.977±0.034	−0.077±0.037	−0.075±0.036
0.771	0.016	0.401	0.500±0.026	0.064±0.051	0.032±0.026
0.732	0.017	0.470	0.263±0.014	0.059±0.079	0.015±0.021
0.691	0.017	0.541	0.138±0.010	0.22 ±0.12	0.031±0.017
0.647	0.018	0.619	0.073±0.012	0.03 ±0.22	0.003±0.016
0.604	0.019	0.694	0.057±0.009	−0.48 ±0.26	−0.027±0.015
0.557	0.019	0.776	0.064±0.009	−0.93 ±0.26	−0.059±0.017
0.511	0.019	0.857	0.099±0.023	−0.99 ±0.36	−0.098±0.035
0.464	0.020	0.939	0.122±0.012	−1.16 ±0.18	−0.142±0.023
0.424	0.039	1.009	0.169±0.014	−0.542±0.084	−0.092±0.014
0.368	0.020	1.107	0.178±0.013	−0.57 ±0.12	−0.102±0.021
0.321	0.020	1.190	0.204±0.012	−0.397±0.088	−0.081±0.018
0.267	0.044	1.284	0.207±0.013	−0.421±0.061	−0.087±0.013
0.181	0.020	1.435	0.224±0.015	−0.20 ±0.09	−0.045±0.021
0.136	0.020	1.514	0.244±0.022	−0.02 ±0.10	−0.005±0.024
0.093	0.020	1.589	0.233±0.018	−0.016±0.090	−0.004±0.021
0.049	0.019	1.666	0.182±0.014	−0.25 ±0.13	−0.046±0.023
0.006	0.028	1.742	0.145±0.010	−0.09 ±0.10	−0.013±0.014
−0.036	0.019	1.815	0.130±0.009	−0.06 ±0.10	−0.008±0.013
−0.059	0.018	1.856		−0.04 ±0.18	−0.004±0.018
−0.086	0.029	1.903	0.077±0.010	−0.12 ±0.17	−0.009±0.013
−0.137	0.032	1.992	0.043±0.006	−0.43 ±0.18	−0.018±0.008
−0.180	0.033	2.068		−1.03 ±0.40	−0.031±0.012
−0.208	0.017	2.117		−0.68 ±0.54	−0.017±0.014
−0.313	0.029	2.301		−0.63 ±0.48	−0.023±0.017
−0.718	0.010	3.010		−0.35 ±1.67	−0.005±0.025
−0.889	0.003	3.310		−0.33 ±0.87	−0.026±0.070

imaginary parts of the forward scattering amplitude.[33] These data were not renormalized.

Besides the well-known forward peak, all the DCS data show a secondary peak at $\cos\theta \approx 0.25$; the secondary peak has a maximum height near 2.07 GeV/c and decreases slowly in magnitude at both the higher and lower energies. In addition, there appears to be a third peak at $\cos\theta \approx -0.4$ which decreases in magnitude with increasing energy and disappears at 2.5 GeV/c. The DCS varies extremely rapidly near 180°, both with

TABLE VI. Experimental results at 2.50 GeV/c.

$\cos\theta_\pi$ (c.m.)	$\Delta(\cos\theta)$	$-t$ [(GeV/c)^2]	$d\sigma/d\Omega$ (mb/sr)	P	$P\,d\sigma/d\Omega$ (mb/sr)
0.908	0.010	0.181	3.89 ±0.50	−0.120±0.030	−0.47 +0.12
0.879	0.012	0.238	2.56 ±0.26	−0.030±0.030	−0.077±0.077
0.846	0.014	0.302	1.565±0.054	−0.048±0.037	−0.075±0.058
0.810	0.014	0.373	0.896±0.035	−0.073±0.050	−0.065±0.045
0.772	0.016	0.448	0.509±0.024	0.285±0.072	0.145±0.037
0.732	0.017	0.526	0.231±0.017	0.34 ±0.12	0.078±0.027
0.689	0.018	0.611	0.121±0.015	0.09 ±0.20	0.011±0.024
0.643	0.019	0.701	0.098±0.014	−0.44 ±0.24	−0.043±0.024
0.597	0.020	0.792	0.080±0.014	−0.98 ±0.32	−0.079±0.026
0.549	0.020	0.886	0.105±0.014	−1.14 ±0.27	−0.119±0.028
0.502	0.020	0.978	0.141±0.018	−0.93 ±0.21	−0.131±0.030
0.448	0.038	1.084	0.166±0.014	−0.56 ±0.12	−0.093±0.020
0.404	0.021	1.171	0.140±0.018	−1.06 ±0.22	−0.148±0.031
0.355	0.021	1.267	0.161±0.018	−0.64 ±0.17	−0.103±0.027
0.286	0.048	1.402	0.192±0.012	−0.404±0.084	−0.078±0.016
0.209	0.020	1.554	0.202±0.017	−0.33 ±0.14	−0.067±0.028
0.162	0.021	1.646	0.142±0.019	−0.60 ±0.20	−0.085±0.028
0.116	0.021	1.736	0.150±0.019	−0.20 ±0.18	−0.030±0.027
0.071	0.021	1.825	0.106±0.015	−0.09 ±0.22	−0.010±0.023
0.040	0.028	1.886	0.109±0.024	−0.38 ±0.25	−0.042±0.027
−0.010	0.028	1.984	0.079±0.011	0.26 ±0.18	0.021±0.014
−0.058	0.019	2.078	0.069±0.018	0.03 ±0.35	0.002±0.024
−0.114	0.029	2.188	0.035±0.016	−0.82 ±0.52	−0.029±0.018
−0.176	0.016	2.310		−1.42 ±0.81	−0.035±0.020
−0.206	0.032	2.369	0.054±0.032	0.31 ±0.57	0.016±0.031
−0.233	0.015	2.422		0.73 ±1.15	0.015±0.024
−0.339	0.030	2.630	0.024±0.024	0.22 ±0.66	0.008±0.016

---

[33] G. Höhler, G. Ebel, and J. Giesecke, Z. Physik **180**, 430 (1964).

TABLE VII. π^+p results at 1.00 GeV/c.

$\cos\theta_\pi$ (c.m.)	$\Delta(\cos\theta)$	$-t$ $[(\text{GeV}/c)^2]$	$d\sigma/d\Omega$ (mb/sr)	P	$P\ d\sigma/d\Omega$ (mb/sr)
0.679	0.027	0.201	1.56 ± 0.20	0.34 ± 0.13	0.53 ± 0.21
0.559	0.029	0.277	1.39 ± 0.17	0.09 ± 0.13	0.13 ± 0.19
0.432	0.028	0.356	1.31 ± 0.20	0.15 ± 0.17	0.19 ± 0.22

energy and angle. Although it is not shown in Fig. 5, our DCS results agree well in the region of overlap with those of the other groups.[6–11] Thus we are confident in our ability to measure the DCS simultaneously with the polarization, even with the complications of a magnetic field and a dense target consisting mostly of complex nuclei.

At all five momenta the polarization is negative in the forward direction and has a positive peak near the first minimum of the DCS. The most striking feature of the polarization data is the negative dip near $\cos\theta = 0.55$. At 1.70 GeV/c, there is only a trace of the dip; it continuously grows through 2.07 GeV/c, until, at 2.50 GeV/c, the polarization is almost -1.0 at $\cos\theta = 0.55$. The polarization remains negative beyond $\cos\theta = 0.2$, although there are indications that it is going positive at the backward angles. We did not obtain data at the backward angles for two reasons: the low cross section and the lack of running time. Although we do not have data at these angles, severe constraints can be placed on $P\ d\sigma/d\Omega$ because $d\sigma/d\Omega$ is so small. This has been illustrated in Fig. 1 of Ref. 4. The lack of data at small angles is caused by the low range of the recoil proton.

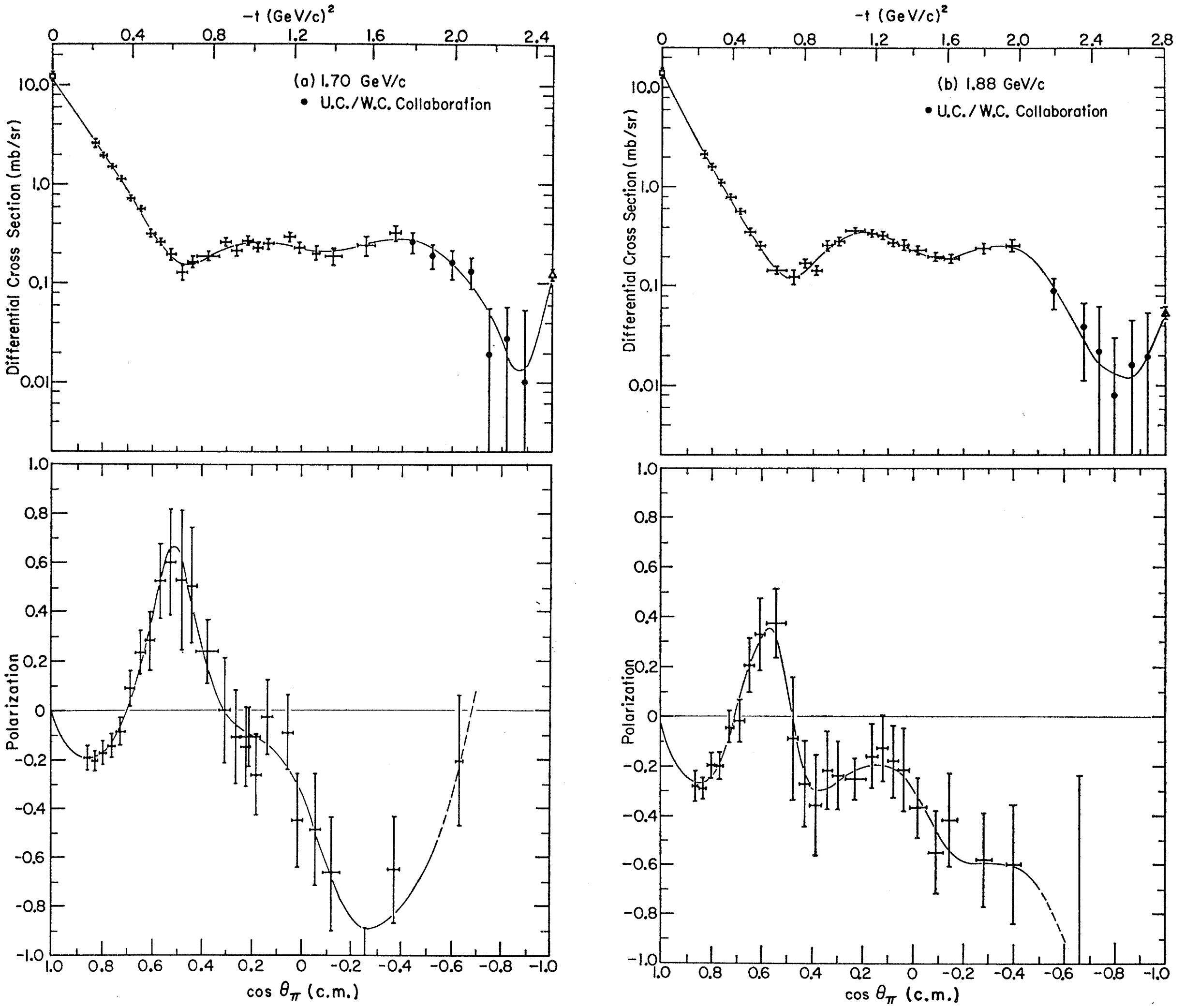

FIG. 5. Differential cross section and polarization in π^-p elastic scattering at (a) 1.70, (b) 1.88, (c) 2.07, (d) 2.27, and (e) 2.50 GeV/c. The curves are the results of fitting the data with the Lengendre series of Eqs. (6) and (7); the vertical bars are statistical errors (1 standard deviation). The horizontal bars show the angular resolution (FWHM).

V. DATA ANALYSIS

A. Legendre Coefficients

We can fit the data in Fig. 5 to Legendre series of the form

$$\frac{d\sigma}{d\Omega}=\bar{\lambda}^2\sum_{n=0}^{N} a_nP_n(\cos\theta)\,, \tag{6}$$

$$P\frac{d\sigma}{d\Omega}=\bar{\lambda}^2\sum_{n=1}^{N} b_nP_n{}^1(\cos\theta)\,. \tag{7}$$

The upper cutoff of the series, N, was determined by the criterion that an increase in N did not appreciably change the χ^2 probability for the fit. The curves in Figs. 5 are the results of the fits and Tables VIII and IX give the corresponding values of a_n and b_n.

In our previous publication[4] we concluded from the energy dependence of these coefficients that the dominant resonant state at 2.07 GeV/c must have $J=l-\frac{1}{2}$ and that the angular momentum $l\leq 4$.

B. Partial-Wave Analysis

In our earlier publication[4] we briefly described a partial-wave analysis of π^-p elastic scattering data in the interval 1.28–2.50 GeV/c. The main result of the analysis reported then was the establishment of the spin-parity of the $N(2190)$ as $J^P=\frac{7}{2}^-$. Since that time the analysis has been repeated independently by one of us (REH) with essentially the same results.

Our analysis has to some extent been superseded recently by the work of three other groups.[34–36] These

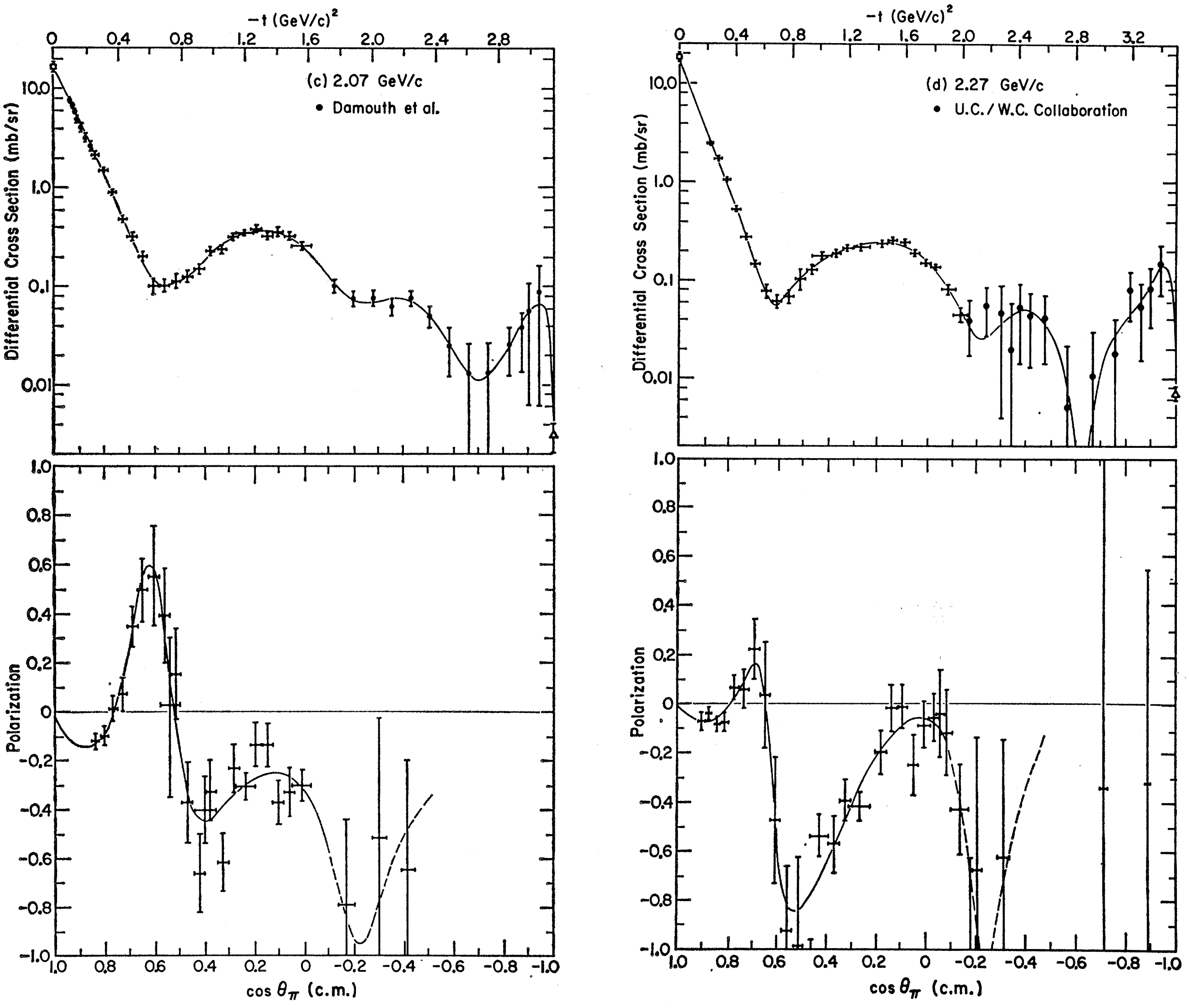

FIG. 5. (*continued*)

---

[34] P. Bareyre, C. Brickman, and G. Villet, Phys. Rev. **165**, 1730 (1968).

[35] A. Donnachie, R. G. Kirsopp, and C. Lovelace, Phys. Letters **26B**, 161 (1968).

[36] C. H. Johnson (Ph.D. thesis), University of California Lawrence Radiation Laboratory Report No. UCRL-17683, 1967 (unpublished).

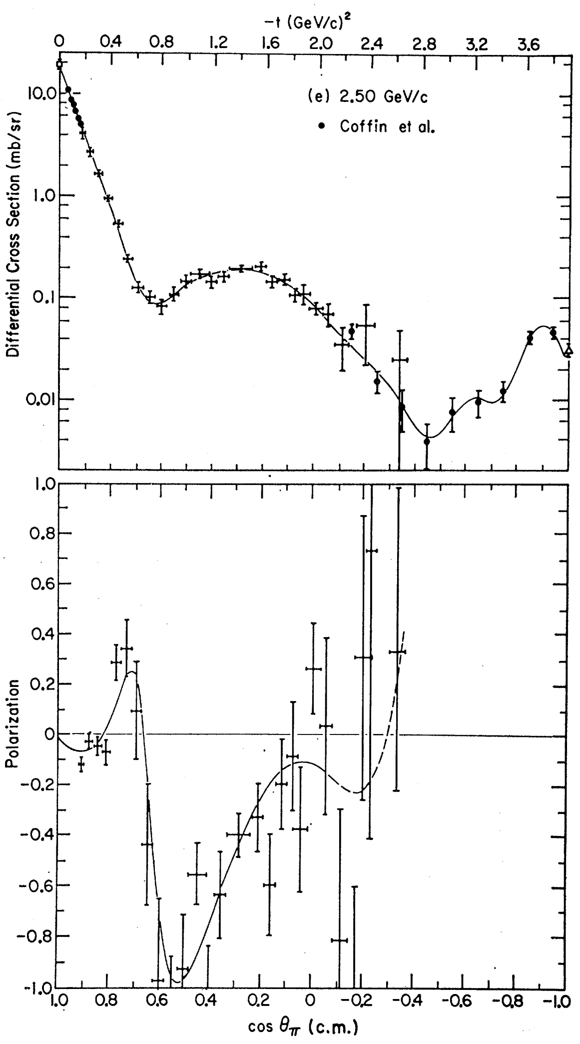

FIG. 5. (*continued*)

groups included new experimental data on π^+p scattering and obtained the $I=\frac{1}{2}$ and $I=\frac{3}{2}$ partial-wave amplitudes separately. In our analysis only π^-p data were used and our partial-wave amplitudes are given by the sum over isospin states, $a(\pi^-p)=\frac{1}{3}(a_{3/2}+2a_{1/2})$. A comparison can be made between our results and the results of the other groups by computing this sum from their partial-wave amplitudes. Such a comparison should be made in the energy region of overlap because phase-shift solutions are inherently ambiguous and independent analyses are desirable to support any claims for uniqueness. Our analysis extends so far to the highest energy and a comparison may contribute to the question of continuity or smoothness at the highest few energies analyzed by the other groups because their results are less certain there. In addition, our analysis reveals some striking features apart from resonances at the higher energies. The isotopic-spin decomposition may not be so relevant at higher energies, and partial-wave amplitudes for π^-p or π^+p scattering (or their symmetric and antisymmetric combinations) may be just as useful as amplitudes of isotopic spins $\frac{1}{2}$ and $\frac{3}{2}$. We will briefly describe the method of our analysis, present the results, and compare them with those of the other groups. Finally, we will discuss their relationship to Regge-pole and other models of high-energy scattering.

Procedure

The analysis included 430 pieces of π^-p elastic scattering data at eight different momenta between 1.28 and 2.5 GeV/*c*. Besides the data shown in Fig. 5 and described in Sec. IV, the DCS and polarization data of the authors of Ref. 7 were used at 1.28, 1.44, and 1.58 GeV/*c*.

The basic method of this analysis was to start with the earlier low-energy solutions[37–41] (in particular, the

TABLE VIII. Legendre coefficients of least-squares fit to $d\sigma/d\Omega=\lambda\!\!\!^{-2}\sum a_nP_n(\cos\theta_\pi)$.

	1.70 GeV/*c*	1.88 GeV/*c*	2.07 GeV/*c*	2.27 GeV/*c*	2.50 GeV/*c*
a_0	1.293±0.014	1.399±0.009	1.524±0.011	1.450±0.068	1.649±0.007
a_1	2.78 ±0.15	3.13 ±0.17	3.67 ±0.13	3.58 ±0.20	4.267±0.071
a_2	3.46 ±0.22	3.94 ±0.26	4.81 ±0.20	4.97 ±0.31	5.95 ±0.11
a_3	3.81 ±0.25	4.56 ±0.31	5.43 ±0.26	5.64 ±0.39	6.77 ±0.15
a_4	3.10 ±0.26	4.23 ±0.32	5.53 ±0.29	6.03 ±0.44	7.08 ±0.17
a_5	1.98 ±0.24	3.13 ±0.30	4.56 ±0.31	5.29 ±0.46	6.40 ±0.20
a_6	1.26 ±0.20	2.18 ±0.27	3.08 ±0.31	4.00 ±0.45	4.95 ±0.21
a_7	0.48 ±0.17	1.22 ±0.24	1.88 ±0.30	2.76 ±0.41	3.49 ±0.21
a_8	0.24 ±0.12	0.67 ±0.20	1.26 ±0.28	1.88 ±0.36	2.28 ±0.21
a_9	0.26 ±0.09	0.59 ±0.17	1.01 ±0.25	1.44 ±0.30	1.52 ±0.20
a_{10}	0.15 ±0.08	0.29 ±0.13	0.50 ±0.21	0.80 ±0.24	0.89 ±0.17
a_{11}		−0.11 ±0.10	0.19 ±0.16	0.46 ±0.18	0.49 ±0.14
a_{12}		−0.11 ±0.08	0.17 ±0.13	0.31 ±0.14	0.27 ±0.11
a_{13}			0.191±0.085	0.252±0.087	0.148±0.077
a_{14}			0.063±0.068	0.001±0.076	0.104±0.041
$P(\chi^2)$ (%)	28	63	73	65	86

---

[37] P. Bareyre, C. Brickman, A. V. Stirling, and G. Villet, Phys. Letters **18**, 342 (1965).

[38] B. H. Bransden, P. J. O'Donnell, and R. G. Moorhouse, Phys. Rev. **139**, B1566 (1965).

[39] A. Donnachie, A. T. Lea, and C. Lovelace, Phys. Letters **19**, 146 (1965).

[40] J. Cence, Phys. Letters **20**, 306 (1966).

[41] L. D. Roper, R. M. Wright, and B. T. Feld, Phys. Rev. **138**, B190 (1965); **138**, B921 (1965).

TABLE IX. Associated Legendre coefficients of least-squares fit to $P\, d\sigma/d\Omega = \lambda\!\!\!^{-2} \sum b_n P_n{}^1(\cos\theta_\pi)$.

	1.70 GeV/c	1.88 GeV/c	2.07 GeV/c	2.27 GeV/c	2.50 GeV/c
b_1	−0.187±0.024	−0.232±0.023	−0.153±0.018	−0.105±0.016	−0.118±0.014
b_2	−0.042±0.027	−0.118±0.026	−0.087±0.021	−0.068±0.017	−0.102±0.016
b_3	−0.097±0.027	−0.152±0.024	−0.063±0.023	−0.036±0.017	−0.057±0.019
b_4	−0.195±0.026	−0.215±0.025	−0.109±0.024	−0.027±0.017	−0.036±0.017
b_5	−0.127±0.028	−0.168±0.026	−0.130±0.023	−0.043±0.017	−0.063±0.018
b_6	−0.065±0.024	−0.126±0.021	−0.109±0.019	−0.052±0.014	−0.089±0.016
b_7	−0.057±0.016	−0.093±0.016	−0.076±0.015	−0.051±0.014	−0.089±0.014
b_8	−0.013±0.014	−0.034±0.013	−0.038±0.011	−0.032±0.008	−0.064±0.021
b_9	+0.012±0.010	−0.003±0.009	−0.009±0.009	−0.001±0.008	−0.032±0.009
b_{10}					−0.012±0.007
$P(\chi^2)$ (%)	99	99	84	94	10

ones of the Saclay group[37]) and proceed upward in energy using a variety of starting sets to obtain a number of possible solutions at each energy. These single-energy solutions were then formed into families of solutions which showed smooth energy dependence in all (or the highest number of) the partial-wave amplitudes a_J, looking at the real and imaginary parts separately. New starting sets were usually employed at this stage. This smoothing and grouping was done by the laborious or visual method (the approach being essentially the same as that employed by the Saclay group[34,37]). No *a priori* assumption about the behavior (or existence) of the higher partial waves was employed; the values of $l_{\max}$ were determined empirically from the Legendre-series fits to the data. This work differs from the analysis previously described[4] in that $l_{\max}$ was the same for both the real and imaginary parts; i.e., the standard partial-wave formalism was employed.

The parameters used were $\delta_l{}^{\pm}$ and $\eta_l{}^{\pm}$ in order to impose unitarity for the partial-wave amplitudes

$$a_l{}^{\pm} = [\eta_l{}^{\pm} \exp(2i\delta_l{}^{\pm}) - 1]/2ik\,.$$

Fits were obtained by minimizing χ^2 with the $2(2l_{\max}+1)$ parameters by the computer program MINFUN. Errors in the δ's and η's and in the partial-wave amplitudes and other quantities of interest were calculated numerically using the complete error matrix generated by MINFUN.

We first confirmed the $\pi^- p$ amplitudes calculated from the solution of Bareyre *et al.*[37] at 1.08 GeV/c, the highest momentum fitted by them. Sets of starting values for the parameters at higher momenta were of three main types: (a) solutions from an adjacent energy, (b) extrapolations from adjacent energies, and (c) "smoothed" solutions. At lower energies, types (a) and (b) were used as starting points for exploratory searches which looked for nearby relative minima.

At higher energies, type-(a) sets usually spanned enough of the parameter space that they were sufficient to locate possible solutions and type-(b) sets were not usually employed. The type-(c) sets were solutions with already good values of χ^2 but which would be better candidates for a "smooth family" if one or more "kinks" could be straightened out—in other words, a previous solution with one or two parameters changed to improve its continuity. The sets were used to try to find the smoothest family of solutions. No completely random searching was attempted.

The sensitivity of solutions to the normalization of the target polarization P_T was checked by calculating $P(\theta)$ from each solution and performing a one-parameter normalization fit to the experimental polarization data. The normalization parameter N is of course guaranteed to be close to unity but the significant quantity is ΔN. We found that all the polarizations at different energies stay within their quoted normalization uncertainty (see Table X) without changing χ^2 by more than 1 or 2.

TABLE X. Goodness of fits.

			Partial-wave analysis			Polarization normalization check		
P_{lab} (GeV/c)	$E_{\text{c.m.}}$ (MeV)	$l_{\max}$	No. of data points	No. of deg of freedom	χ^2 (total)	No. of pol'n points	χ^2 (pol'n)	Normalization factor
1.28	1821	4	36	18	31.9	16	9.1	1.02±0.11
1.352[a]	1857					23	10.8	1.02±0.05
1.44	1901	4	36	18	21.3	16	4.8	1.01±0.12
1.58	1970	4	36	18	23.3	16	9.6	1.00±0.18
1.70	2025	4	59	41	49.4	26	8.5	0.97±0.08
1.88	2106	5	57	35	34.7	25	5.7	1.00±0.08
1.988[a]	2154					24	11.1	1.01±0.06
2.07	2189	5	68	46	48.2	25	17.6	1.00±0.07
2.27	2272	6	69	44	64.9	30	23.1	1.01±0.07
2.50	2366	6	69	43	67.3	27	35.6	1.03±0.08
2.535[a]	2380					16	14.8	1.00±0.09

[a] Polarization data from Ref. 14.

Results

From Legendre-polynomial fits to the differential cross sections, values of $l_{\max}$ were found to increase in the interval 1.28–2.50 GeV/c from 4 to 6. These values give a radius of interaction R (given by a semiclassical model as $R=\lambda\!\!\!^{-} l_{\max}$) of between 1.0 and 1.2 F.

At each energy a number of acceptable solutions were found for the partial-wave amplitudes. On the basis of the smoothness requirement discussed in the preceding section, there seemed to be one distinctly superior family between 1.28 and 1.70 GeV/c which also appeared to be a reasonable extrapolation of the

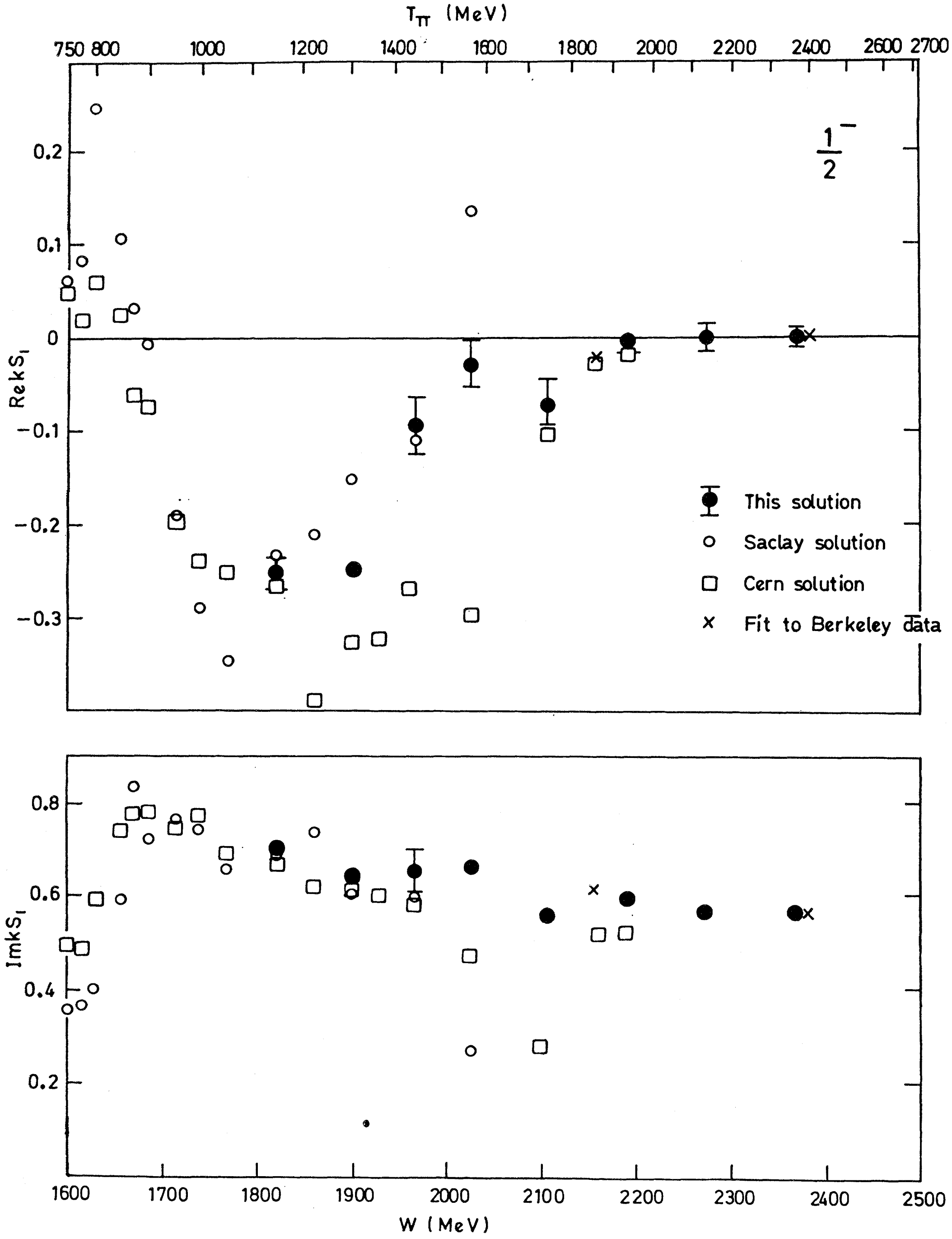

FIG. 6. Partial-wave amplitudes as a function of the total c.m. energy W. The open circles are from Ref. 34, the open squares are from Ref. 35, and the crosses are our amplitudes derived from the data of Ref. 14.

solutions at lower energies. At higher momenta the distinction between the smoothness of possible families became less clear. The family of solutions presented here appeared to be somewhat superior in its over-all smoothness compared to the other possible ones. We do not attempt to express quantitatively the degree of superiority since, in the end, selection was made on the basis of personal judgment. This family constitutes an acceptable fit to the data at each momentum. The total χ^2 is 341, giving an average χ^2 per degree of freedom of 1.3. The goodness-of-fit information is summarized in Table X together with results of the normalization check of the polarization data.

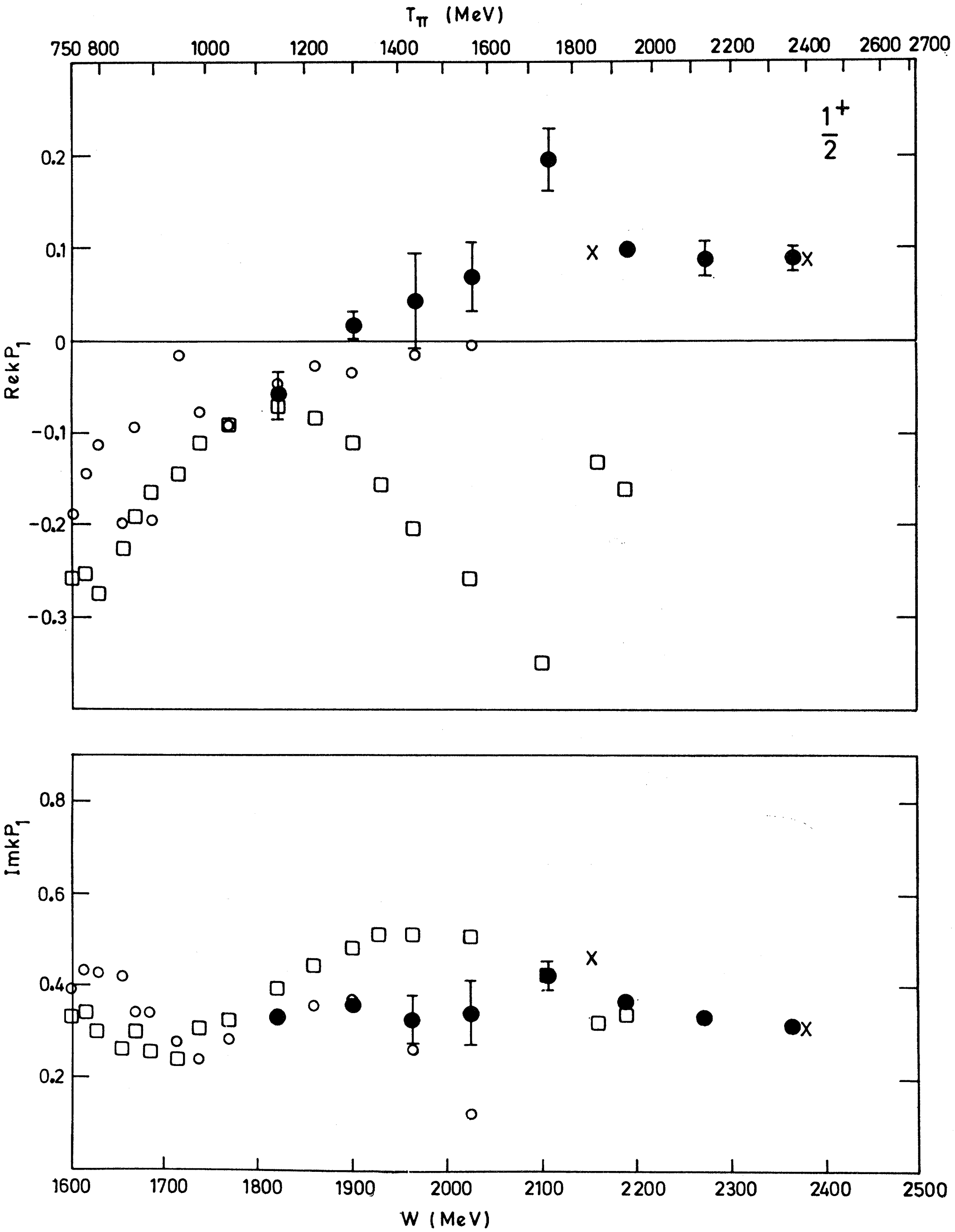

FIG. 6. (*continued*)

Partial-Wave Amplitudes

The partial-wave amplitudes obtained are shown as the solid circles in Figs. 6, where we have plotted the real and imaginary parts separately as functions of W, the total energy or "mass" in the c.m. system. In these figures the amplitudes are denoted by L_{2J}, where L denotes the orbital angular momentum state (S, P, D, etc.) and J the total angular momentum. A Breit-Wigner resonance of mass M would ideally appear in these plots as shown in Fig. 7, where we show the real and imaginary parts of $kL_{2J}=cx\Gamma[2(M-E)-i\Gamma]^{-1}$. Here $x=\Gamma_e/\Gamma$ is the elasticity of the resonance and c

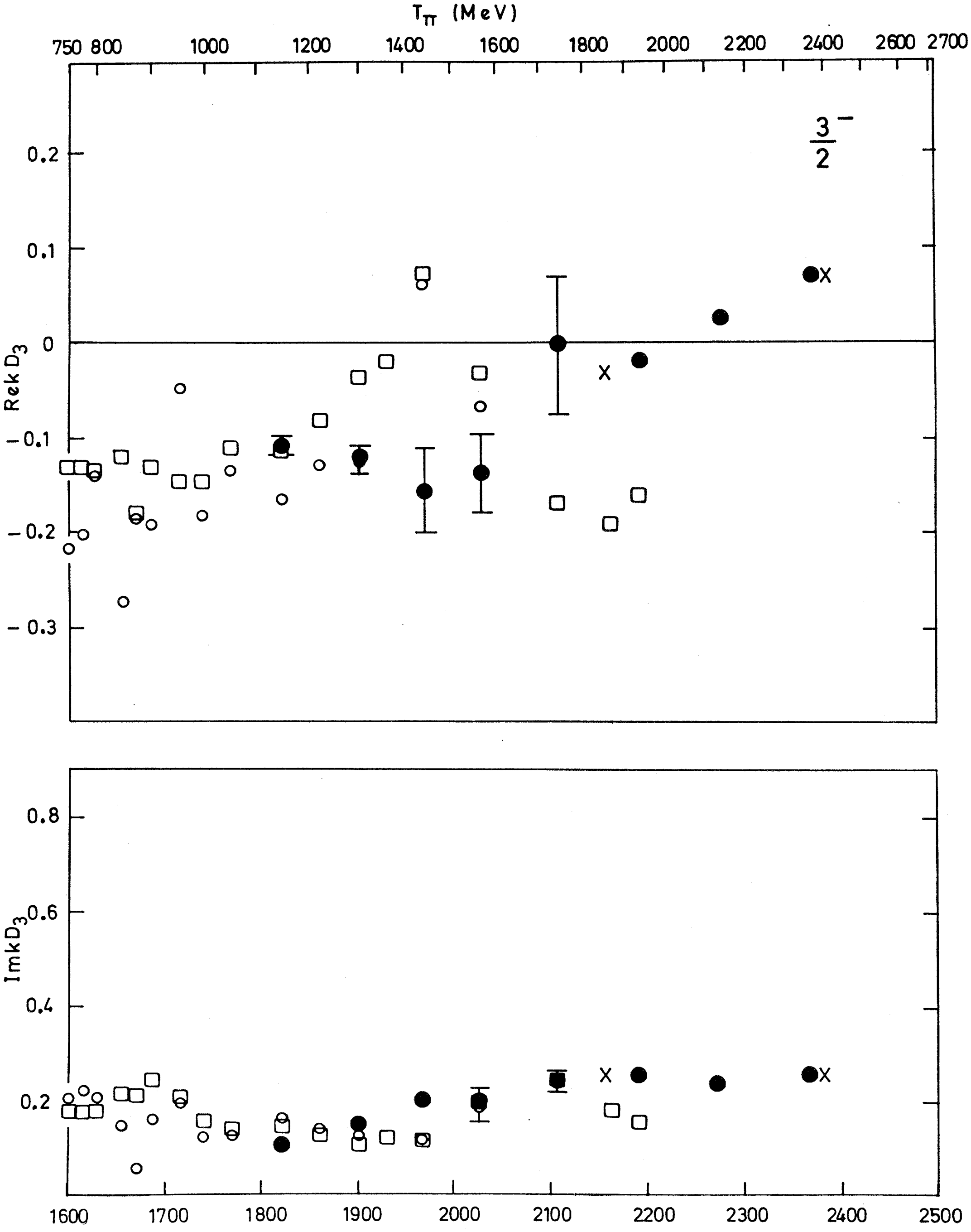

FIG. 6. (*continued*)

is the appropriate Clebsch-Gordan coefficient: $\frac{1}{3}$ for $I=\frac{3}{2}$ or $\frac{2}{3}$ for $I=\frac{1}{2}$. This idealized behavior is in practice modified by threshold effects and by the background or nonresonant contribution to the partial-wave amplitude. For our $\pi^- p$ amplitudes there is the additional background from the other isospin state.

In addition to the solid circles in Figs. 6 which represent our solution, there are crosses which fit the Berkeley $\pi^- p$ polarization data at 1.988 and 2.535 GeV/c.[14] Also shown are boxes and open circles which indicate the $\pi^- p$ amplitudes calculated from the phase-shift solutions above 900 MeV/c of the CERN and

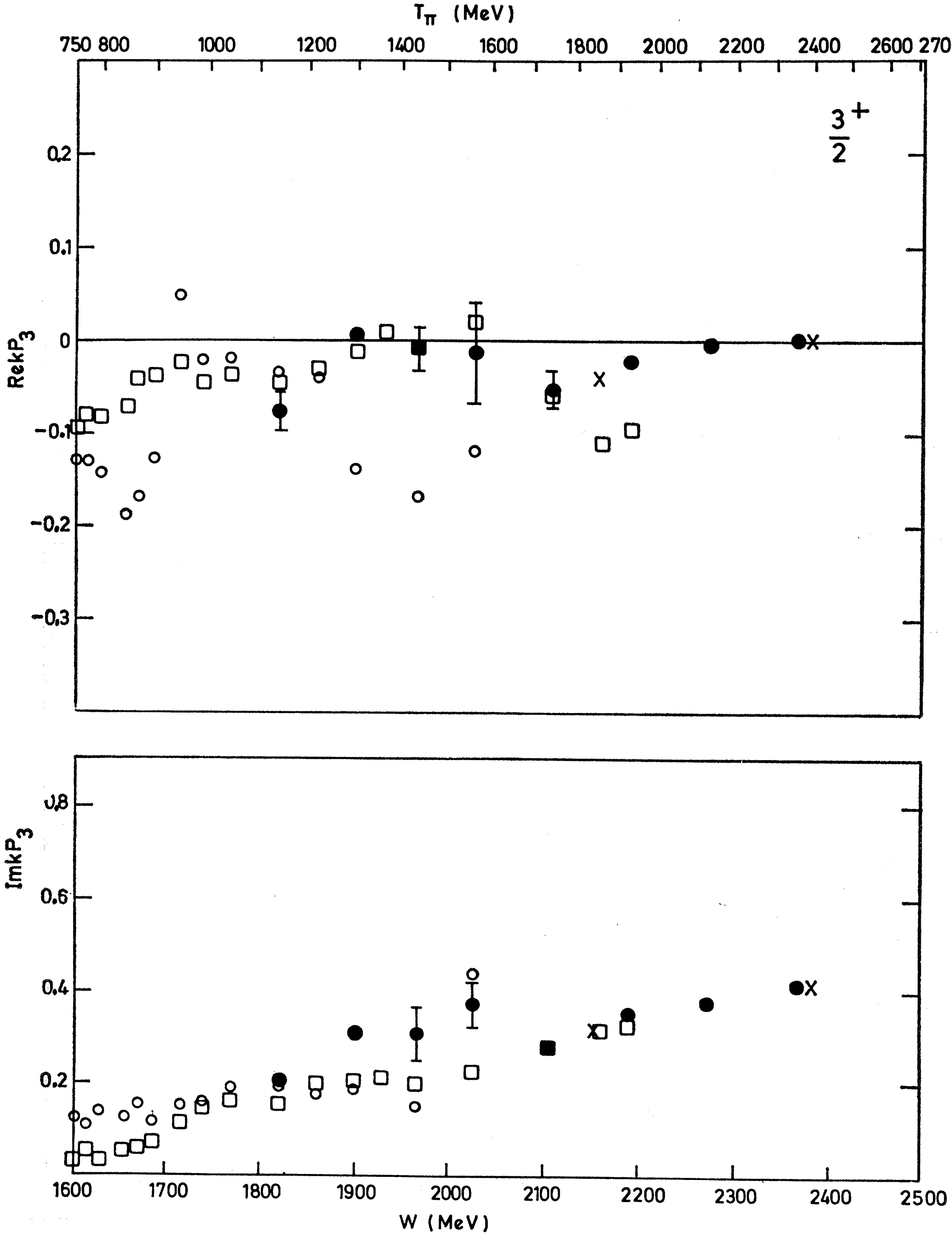

Fig. 6. (*continued*)

Saclay groups, respectively. These will be discussed in more detail below. Here, we will make a few comments on the partial-wave amplitudes of our solution.

S_1. Both S_{31} and S_{11} resonate at around 1700 MeV,[34] and ReS_1 is seen to go negative very rapidly. At higher energies ReS_1 gradually approaches zero. After peaking at about 1700 MeV, ImS_1 drops off more slowly on the high-energy side and appears to become constant.

P_1. The behavior near 2100 MeV is consistent with the presence of a resonance of mass $\simeq$2160 MeV and $cx \simeq 0.1$, although the evidence in the real part is given almost entirely by the 1.88-GeV/c data.

P_3. Here the behavior is rather smooth, with the real

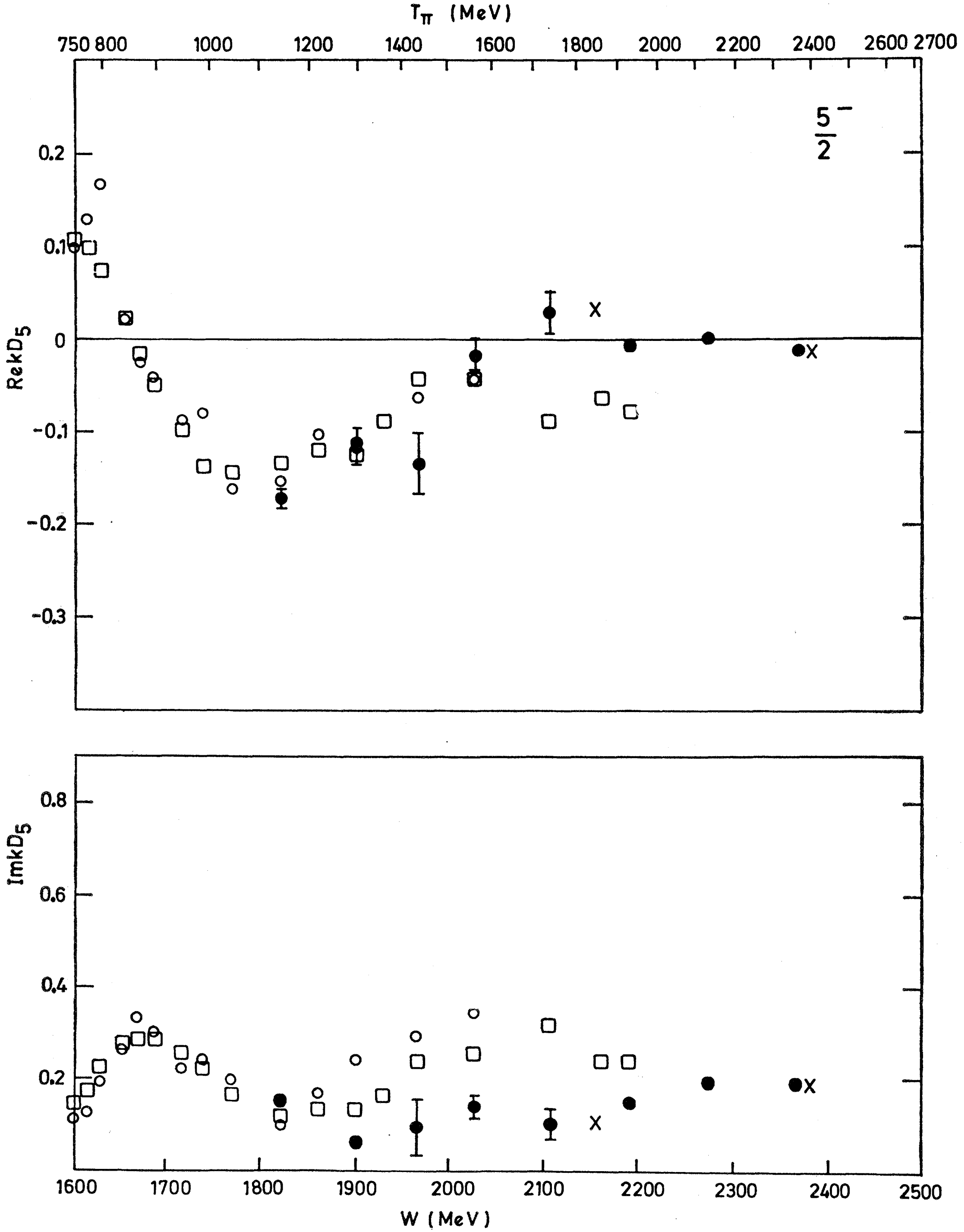

FIG. 6. (*continued*)

part gradually approaching zero and the imaginary part leveling off after an initial rise.

D_3. The real part shows no sign of leveling off and, after becoming attractive at about 2220 MeV, continues to increase. The imaginary part appears to be leveling off after slowly increasing from a minimum on the high side of the $D_{13}(1520)$.

D_5. Our solution shows nothing remarkable above the $D_{15}(1700)$. The real part tends to be small and the imaginary part rather constant.

F_5. The situation here is almost identical to D_5, except that the real part is staying more negative at higher energy.

F_7. The behavior here is dominated by the $\Delta(1920)$,

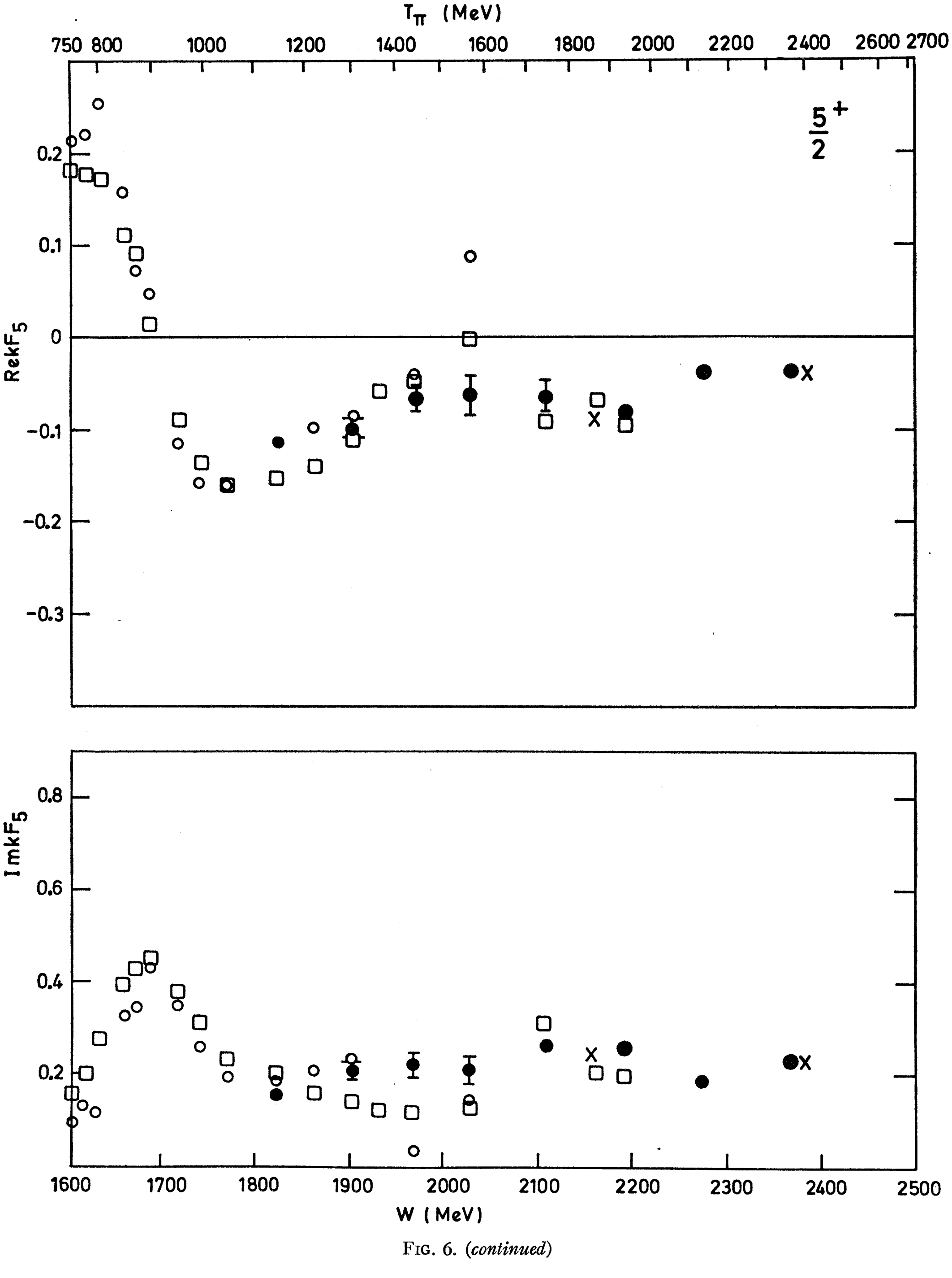

FIG. 6. (*continued*)

which appears strongly in the $\pi^- p$ amplitude. This solution shows almost a classic resonance behavior with a mass ~1940 MeV and elasticity $\simeq 0.5$ (for $I=\frac{3}{2}$). Note that in our solution the imaginary part becomes small above resonance before increasing again.

G_7. A G_{17} resonance is clearly indicated here, although the behavior is far from classic. There appears to be a strong background contribution to the imaginary part which increases steadily with energy. Our best guess at the mass is 2160 MeV with elasticity ~0.15 (for $I=\frac{1}{2}$).

G_9. The real part shows resonant behavior at 2000 MeV but the imaginary part in our solution shows no corresponding bump.

H_9. The real part is consistent with zero, while the imaginary part steadily increases.

H_{11}. The situation is identical to H_9 except that the

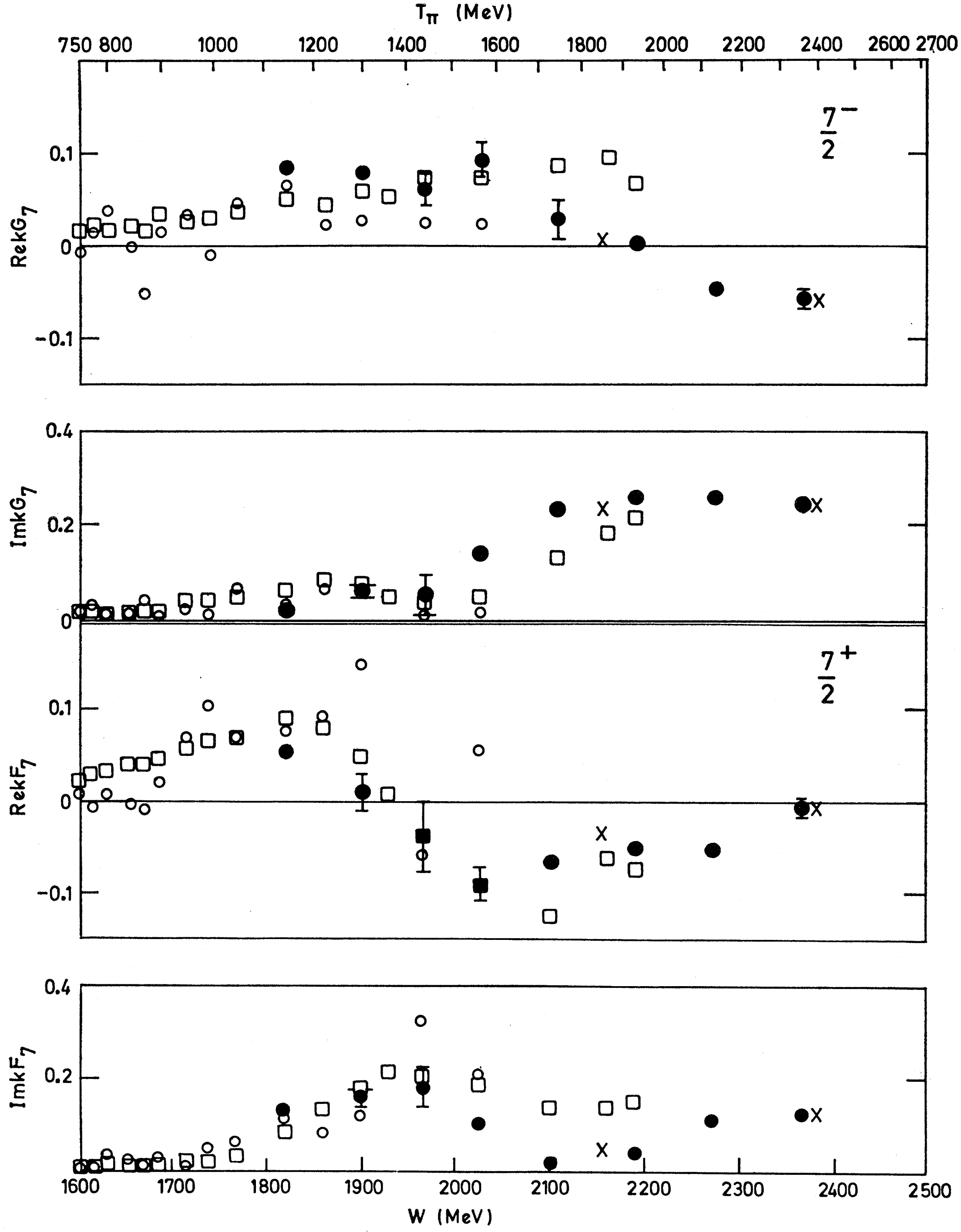

FIG. 6. (*continued*)

imaginary amplitude at 2.50 GeV/c shows a small decrease, thereby giving rise to a speculative $11/2^+$ resonance at $\simeq$2240 MeV with $cx\simeq0.05$. This solution does not give support to the claim for an $11/2^+$ assignment for the Δ(2420).[42]

Higher waves. If any higher wave resonates soon after 2.50 GeV/c, it would probably be the $11/2^-$ because of the positive real part.

We have noted for several of the partial-wave amplitudes the tendency of the real part to be small at higher energies, and of the imaginary part to become comparatively constant. This is the sort of behavior one expects

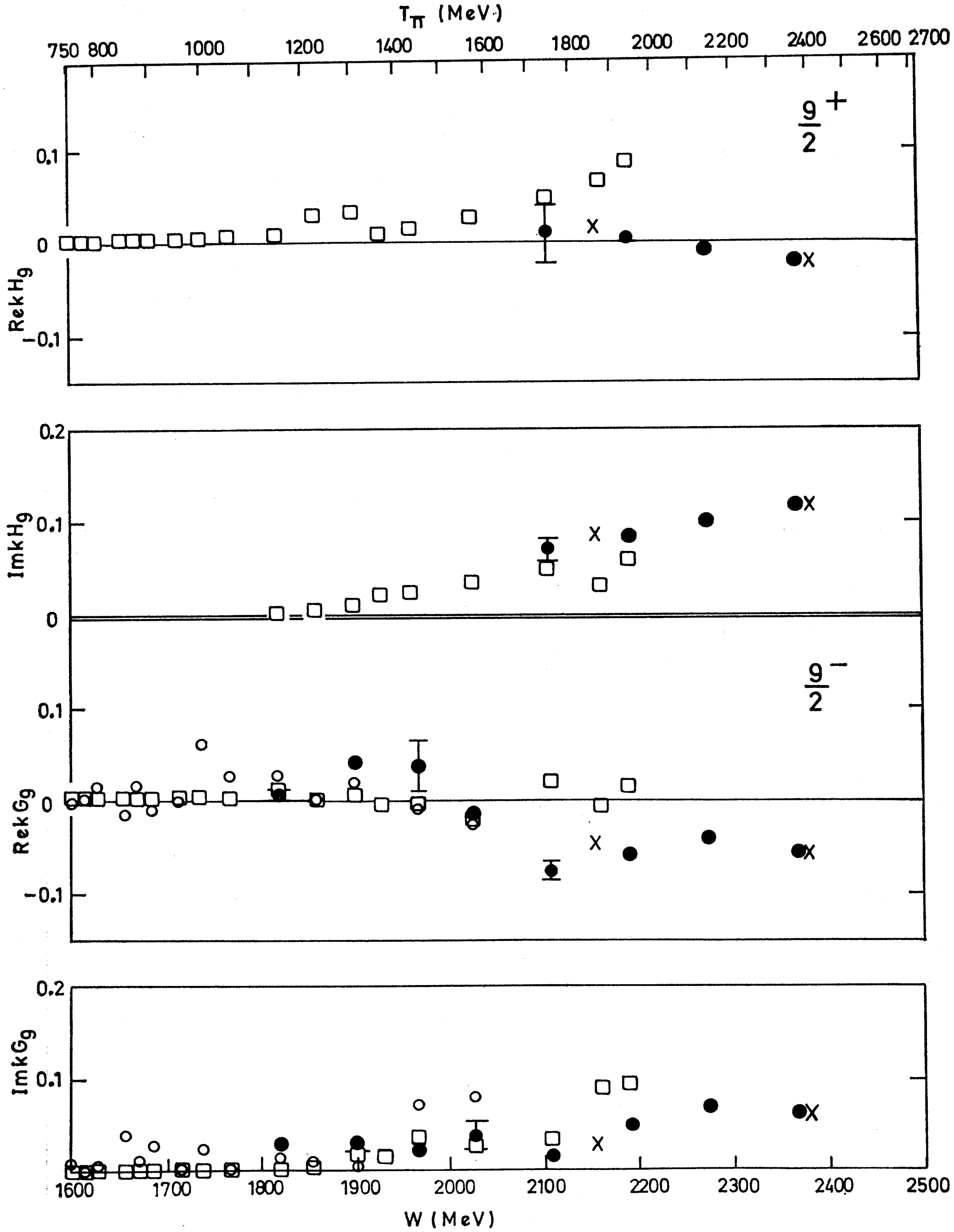

FIG. 6. (*continued*)

---

[42] E. H. Bellamy, T. F. Buckley, R. W. Dobinson, P. V. March. J. A. Strong, R. N. F. Walker, W. Busza, B. G. Duff, D. A, Garbutt, F. F. Heymann, C. C. Nimmon, K. M. Potter, and T. P. Swetman, Phys. Rev. Letters 19, 476 (1967).

from a diffraction model. The tendency for the imaginary parts to become constant may be a result of our selection procedure, which tries to make each partial-wave amplitude a smooth function of energy. However, this method treats each L_{2J} separately and we would not expect that the procedure would give any correlation among the various L_{2J}. However, at the highest energies there does seem to be correlation, at least in the imaginary parts. In Fig. 8 we plot the real and imaginary parts of the amplitudes at 2.50 GeV/c against l, separately for $J=l+\frac{1}{2}$ and $J=l-\frac{1}{2}$. Except for the imaginary part of G_7 which has just resonated, the imaginary parts fall on two smooth curves. Note the strong spin dependence of the imaginary parts.

The smooth l dependence is expected on a diffraction model, or a model in which t-channel exchange is the dominant mechanism. It is not, so far as we can see, expected from our criteria for selecting a solution. The correlation does not seem to exist for the real parts, although we note that in most cases the real parts are

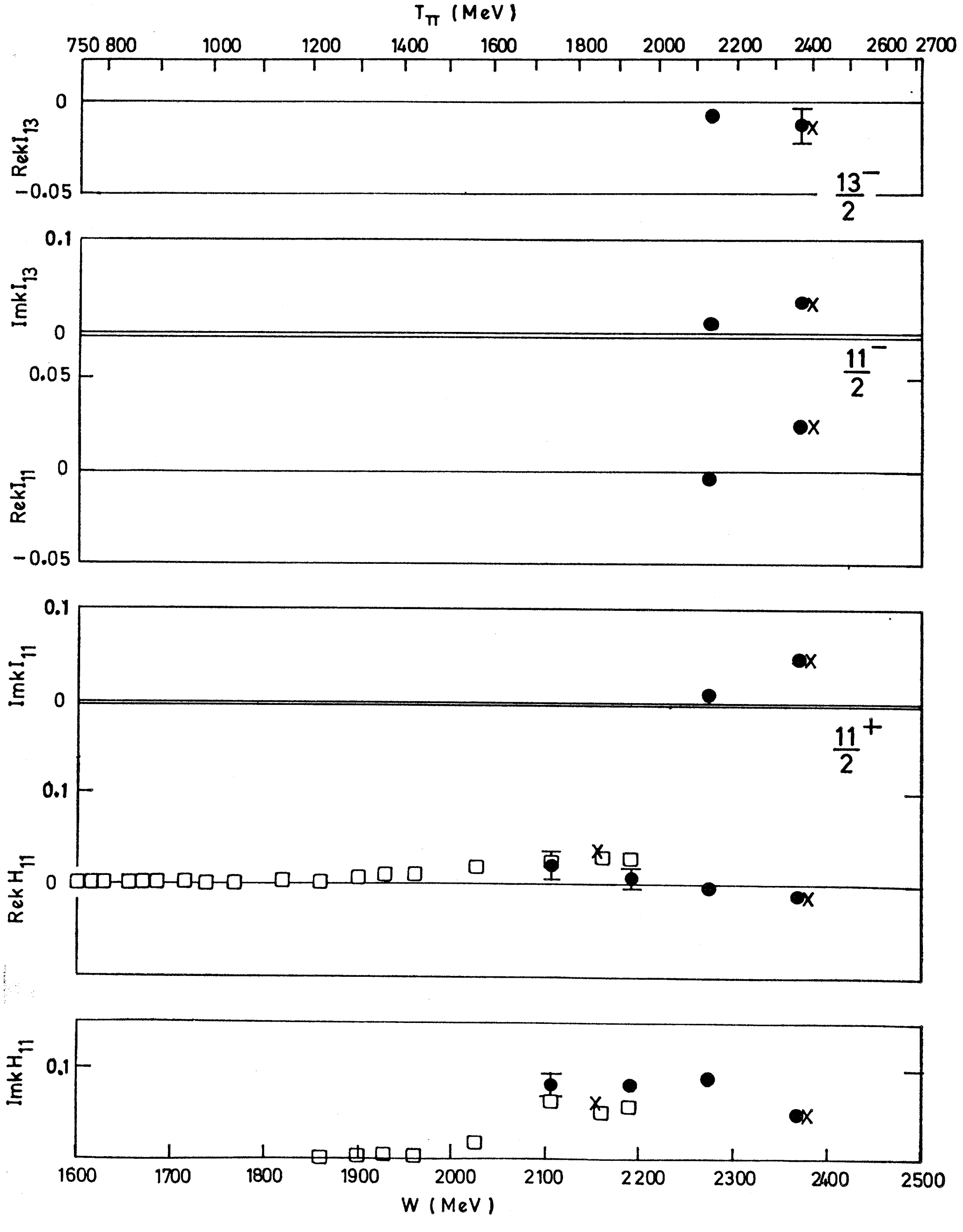

FIG. 6. (*continued*)

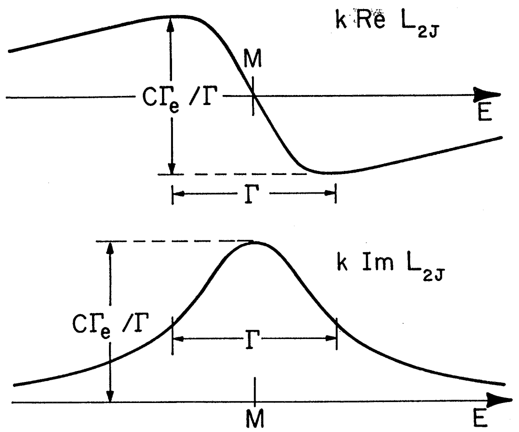

FIG. 7. Partial-wave amplitude behavior of an ideal Breit-Wigner resonance.

much smaller than the imaginary parts (note the different scales). A large part of the transition from resonance-dominated behavior of the amplitudes to the more smoothly energy-dependent behavior characteristic of t-channel exchange takes place in the rather small energy interval of Figs. 6.

Comparison with Other Phase-Shift Solutions

Recently several groups have reported πN phase-shift solutions extending into this energy region.[34–36]

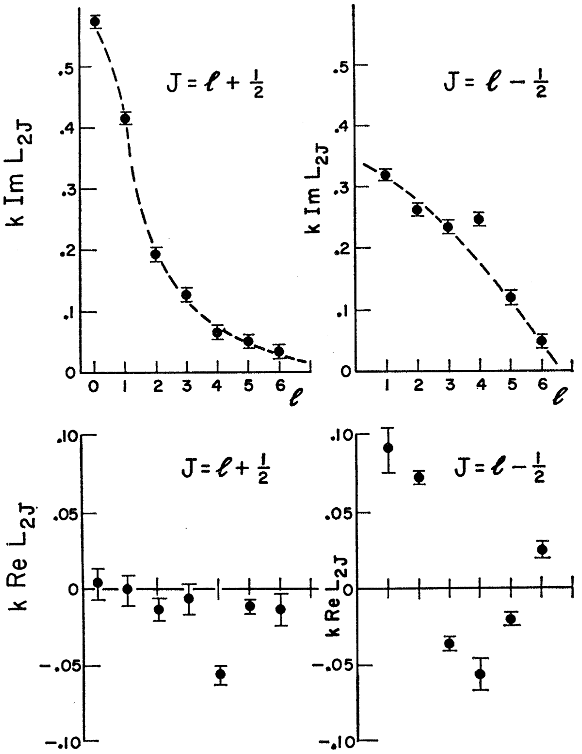

FIG. 8. Partial-wave amplitudes from the phase-shift analysis at 2.50 GeV/c plotted versus l.

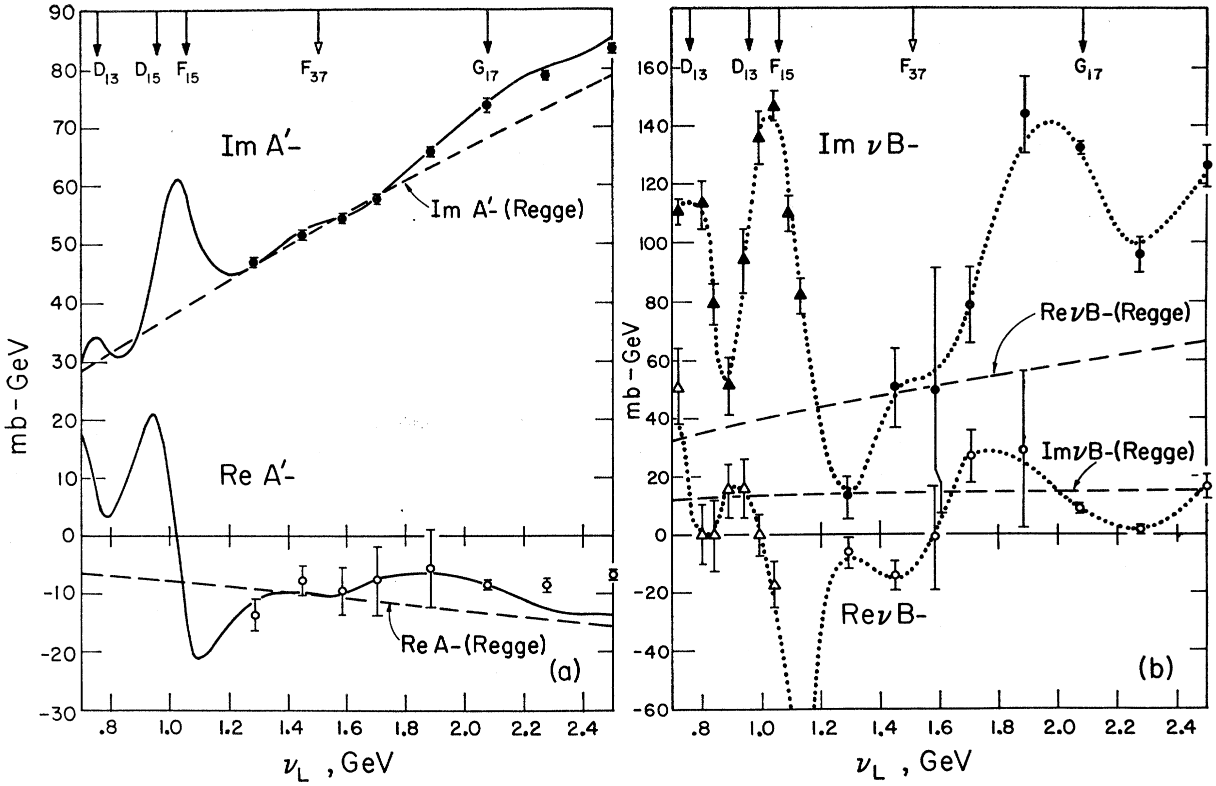

FIG. 9. Real and imaginary parts of the invariant amplitudes (a) A_-' and (b) νB_- versus ν_L. The circular points are derived from our phase-shift solution, the triangular points from Ref. 47, the solid lines from Ref. 33, the dashed lines from Ref. 46; the dotted lines are merely to guide the eye.

The present status of the work of these groups was reviewed by Lovelace in his talk at the Heidelberg Conference,[43] and by Donnachie at the Vienna Conference.[44] Although the present π^-p work is no substitute for a full πN analysis over both isospin states, it is at least relevant to compare the results as a measure of the strength of any claim for uniqueness. This comparison may also contribute to the question of continuity or smoothness, since this analysis is extended to higher energies than the analyses of the other groups.

Comparing the three solutions in Figs. 6, it is seen that this solution is on the whole smoother than those of the other groups. This is, of course, not surprising, since they were smoothing the $\frac{1}{2}$ and $\frac{3}{2}$ amplitudes separately. Of the nine new probable resonances claimed by the CERN group,[35] six are in the energy region of this analysis. Of these six, four are still visible in the CERN π^-p amplitudes; i.e., the resonance behavior has not been obliterated by $\frac{1}{2}$, $\frac{3}{2}$ interference. These four are $F_{35}(1913)$, $P_{31}(1934)$, $D_{35}(\sim 1954)$, and $D_{13}(2057)$; the masses are those given by the CERN group and in some cases they appear to be shifted considerably in energy in the π^-p amplitudes. In each of these four cases, the present solution shows no

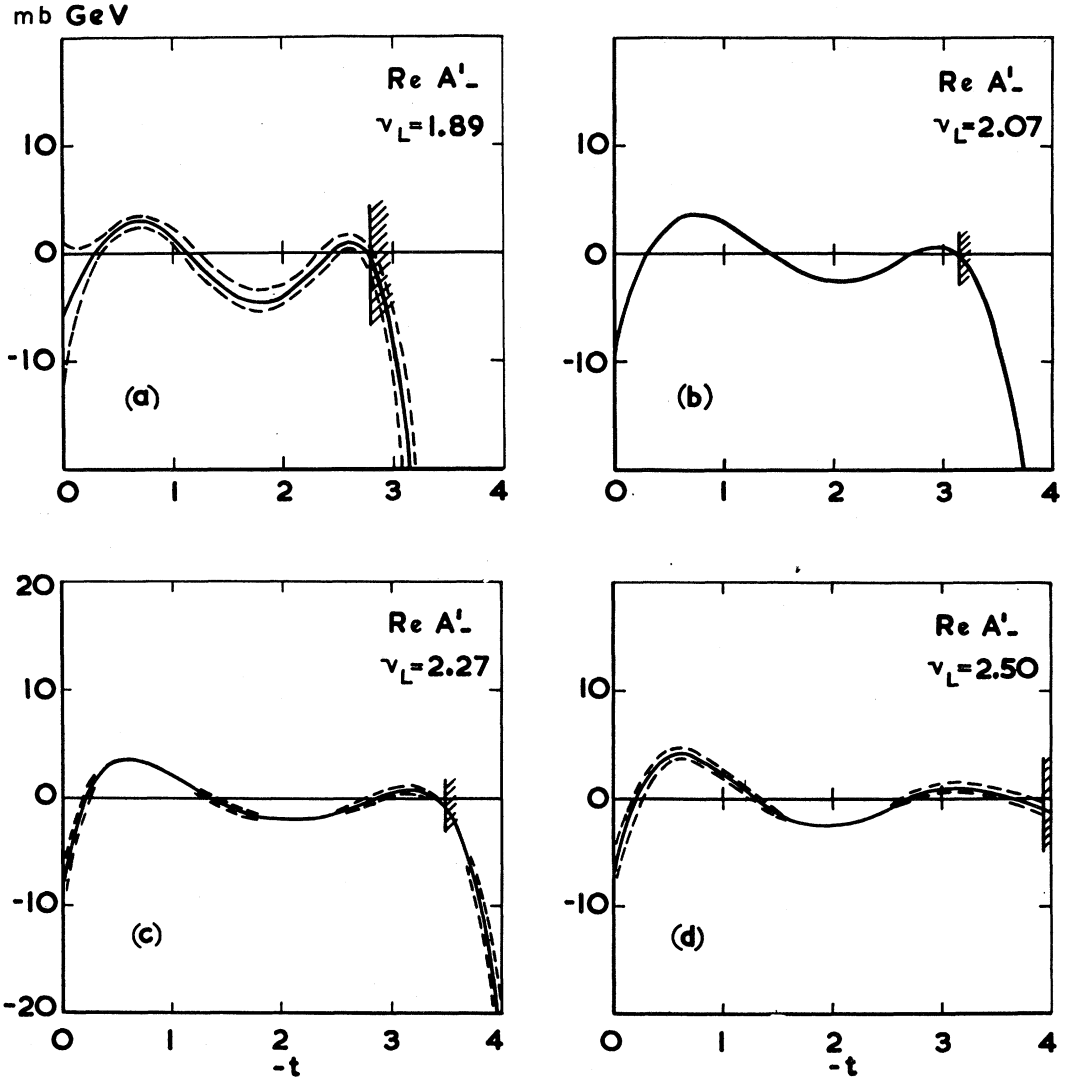

FIG. 10. The t dependence of the real and imaginary parts of A_-' and νB_- at our four highest energies. The dashed lines indicate the range of errors in the amplitudes and the shaded vertical line indicates the kinematical limit of t. The units of t are $(\text{GeV}/c)^2$.

---

[43] C. Lovelace, in *Proceedings of the International Conference on Elementary Particles, Heidelberg*, 1967, edited by H. Filthuth (North-Holland Publishing Co., Amsterdam, 1968), p. 79.

[44] A. Donnachie, in *Proceedings of the Fourteenth International Conference on High-Energy Physics, Vienna, 1968* (CERN, Geneva, 1968), p. 139.

such resonance behavior. We could not expect to distinguish the $F_{17}(1983)$ from the $F_{37}(1940)$ in the π^-p amplitudes.

This solution puts the mass of the $\frac{7}{2}^-$ resonance near 2160 MeV and $c\Gamma_e/\Gamma\sim0.1$. These disagree with the assignments of the CERN group.[34,35] It should be noted that, since their phase-shift solution extends to only 2190 MeV, their assignments must be based on either an energy extrapolation or other evidence. Some of the wobbles in this solution could possibly be explained by highly inelastic resonances, in particular, the wobble in $\frac{1}{2}^-$ near 2040 MeV, in $\frac{1}{2}^+$ near 2160 MeV, in $\frac{9}{2}^-$ near 2000 MeV, and, though highly speculative, in $\frac{11}{2}^+$ near 2240 MeV.

Comparison with Dispersion Relations and Regge Models

From our partial-wave solution we have computed the invariant amplitudes A_- and B_-, using the standard formulas given by Singh,[45] and $A_-'=A_-+\nu B_-(1-t/4m_p^2)^{-1}$, where $\nu=(s-u)/4m_p=\nu_L+t/4m_p$ and ν_L is the total laboratory energy of the incident pion. The total cross section is given by $\sigma_T(\pi^-p)=\mathrm{Im}A_-'(t=0)/p_L$. In Fig. 9(a) we compare the results of our solution to $\mathrm{Im}A_-'$ computed from the smoothed total cross sections computed by Höhler *et al.*[33] We also compare our values of $\mathrm{Re}A_-'$ with the dispersion-relation calculations of Höhler *et al.*[33] The agreement is satisfactory, except perhaps at the highest energy. Also shown as dashed curves are calculations from a typical Regge fit to

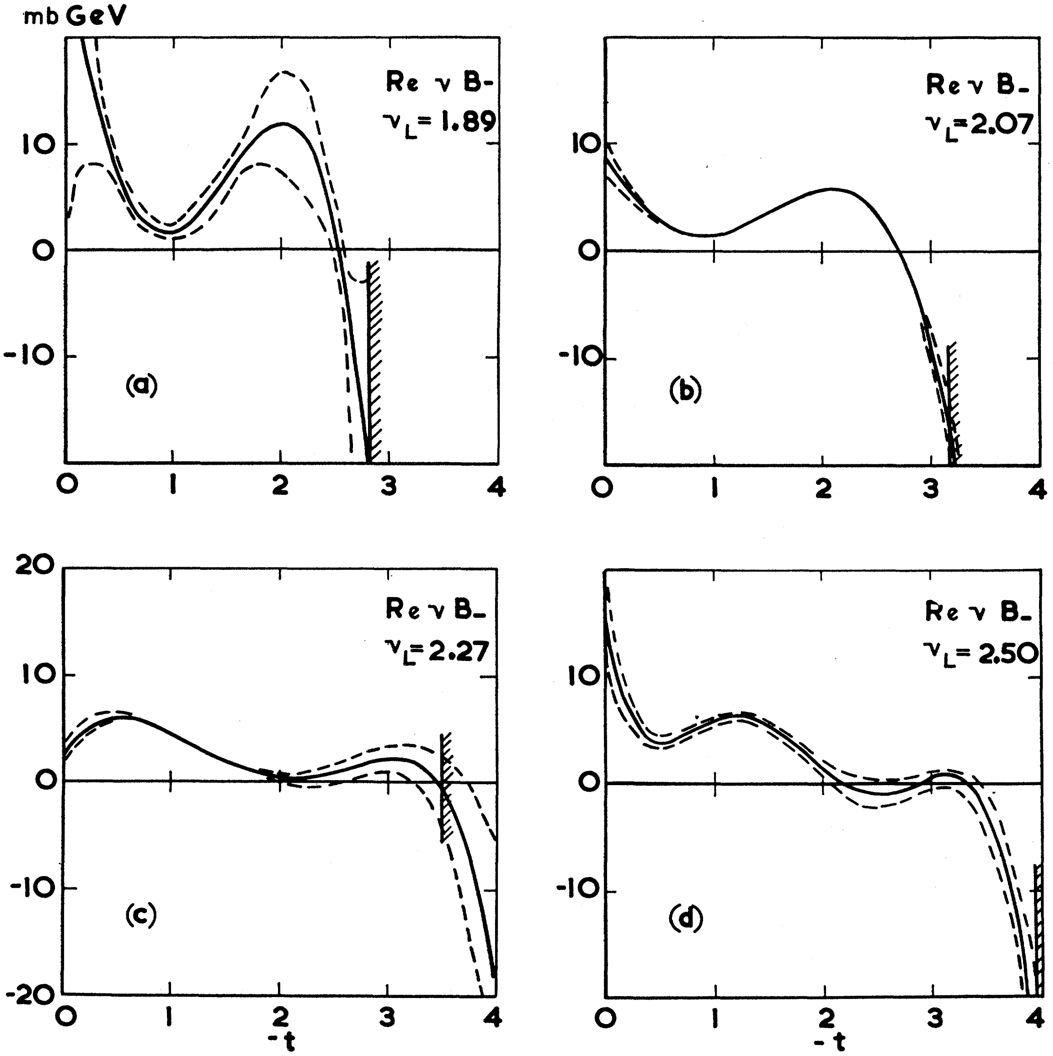

FIG. 10. (*continued*)

---

[45] V. Singh, Phys. Rev. 129, 1889 (1963).

higher-energy data—in this case, solution (b) of Chiu *et al.*[46] Apart from the resonance wiggles, the Regge amplitude gives a qualitatively good extrapolation.

The resonances show up more strongly in B_- as shown in Fig. 9(b). Dispersion relations for $B_\pm$ have been used by Draxler and Hüper to check the consistency of phase-shift solutions at lower energies.[47] The triangular points are their calculations of B_- from the phase-shift solution of Bareyre *et al.*[37]; the circular points are calculated from our phase-shift solution. The dotted lines merely

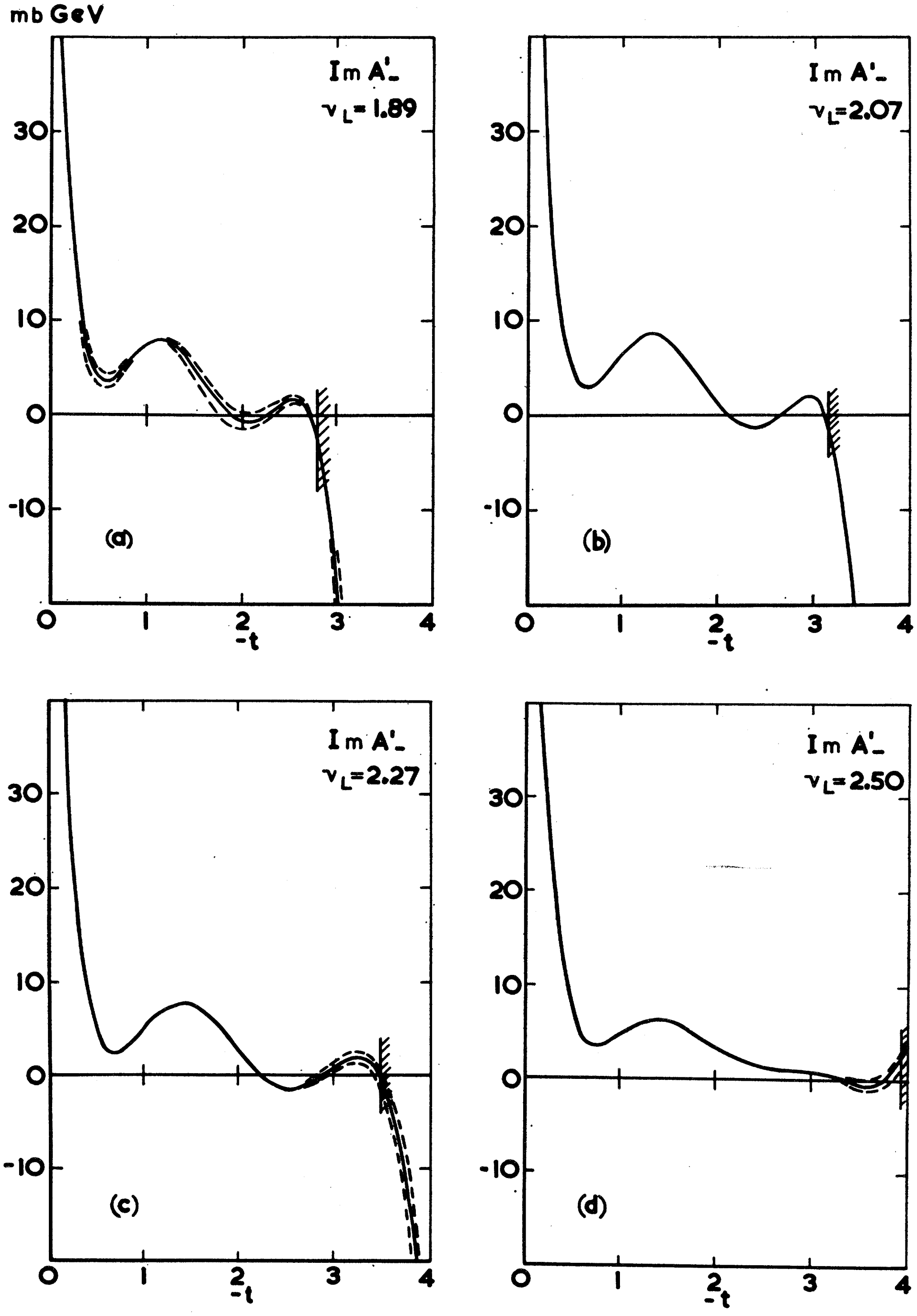

FIG. 10. (*continued*)

---

[46] C. B. Chiu, R. J. N. Phillips, and W. Rarita, Phys. Rev. **153**, 1485 (1967).

[47] K. D. Draxler and R. Hüper, Phys. Letters **20**, 199 (1966).

connect the points. Here the agreement with the extrapolation of Regge-pole parametrizations is not so good as for A_-'. The dashed curves are calculated from solution (b) of Chiu *et al.*[46]; their solution (a) gives Im$\nu B_- = -236$ mb GeV at $\nu_L = 2.5$ GeV, in complete disagreement with our phase-shift solution. Some of the more recent parametrizations should give better agreement. In particular, it has been realized that νB_- should be positive.

t Dependence of A' and B

In Figs. 10 we show the t dependence of A_-' and B_- at the four highest energies $\nu_L = 1.89$, 2.07, 2.27, and

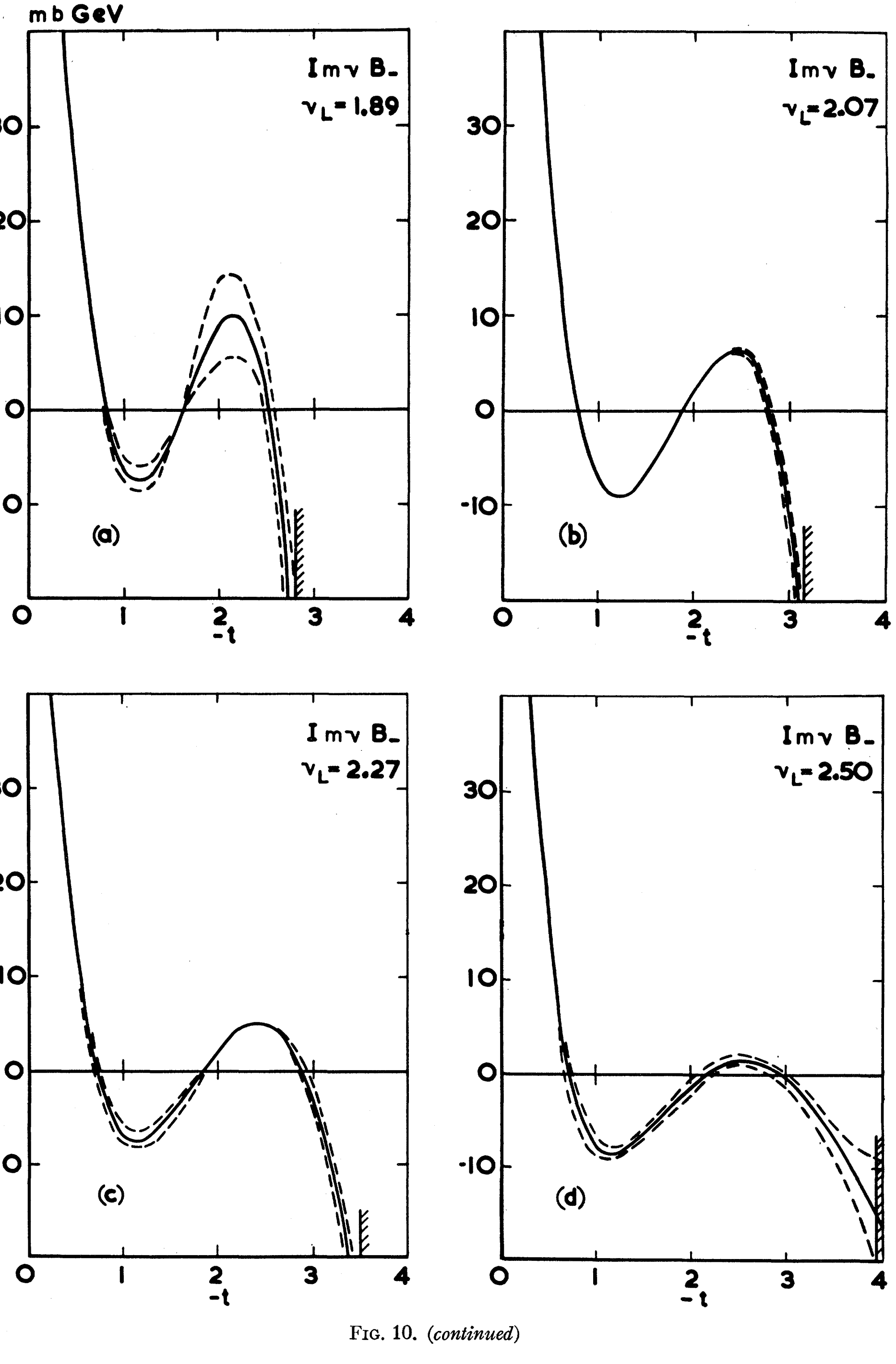

FIG. 10. (*continued*)

2.50 GeV. The dip in the differential cross sections at $-t\approx 0.8$ and the secondary maximum at $-t\approx 1.2$ are clearly associated with the structure of $\text{Im}A_-'$ and with the zero and negative maximum of $\text{Im}\nu B_-$. Because of the kinematic factors involved in calculating the cross section from A_-' and νB_-, A_-' accounts for about $\frac{2}{3}$ and νB_- for about $\frac{1}{3}$ of the secondary maximum.

Both the real and imaginary parts of A_-' and $\text{Im}\nu B_-$ change very little in the energy range shown. Only $\text{Re}\nu B_-$ appears to change markedly with ν_L. It may be reasonable to expect that any stationary behavior observed in the amplitudes will persist at higher energies. For example, the first dip in $\text{Im}A_-'$ occurs at $-t=0.6$–0.8 from $\nu_L=1.6$ to 2.5 GeV, and the secondary maximum occurs between $-t=1.2$ and 1.5. Differential cross sections at higher energies show this same t dependence, but with the secondary maximum gradually disappearing.

The first zero in $\text{Re}A_-'$ occurs at $-t\approx 0.6$ at the lowest energy of our analysis but moves in to smaller $-t$ as the energy increases and levels off at $-t\approx 0.2$. This may be associated with the crossover effect of the π^+p and π^-p cross sections which is observed at $-t\approx 0.2$ at higher energies. The second zero appears to be somewhat stationary, being always between $-t=1.1$ and 1.7 from $\nu_L=1.3$ to 2.5 GeV. The location of the third zero moves steadily in $-t$ as the energy increases, but shows an indication that it may become stationary at $-t\approx 3$.

The first zero in $\text{Im}\nu B_-$ remains between $-t=0.6$ and 0.8 above $\nu_L=1.6$ GeV and, above this energy, two other zeros form which move to larger $-t$ as the energy increases. The second of these may become fixed at $-t\approx 3$ at higher energies.

Agreement with Subsequent Experiments

We have compared our partial-wave solution to some more recent data (for example, the backward DCS data of Carroll *et al.*[8]) which were not used in the analysis and found the results to be in satisfactory agreement within the errors. Also, our solution has been compared[48] with new polarization data from the Rutherford High-Energy Laboratory[49] and found to be in good agreement. The agreement is not surprising, since the RHEL polarization measurements agree with those reported here. Also recent measurements of the DCS up to 2.5 GeV/c are in generally good agreement with our experimental results.[50]

Summary of Conclusions

We have reported measurements of the cross section and polarization in π^-p elastic scattering at five momenta between 1.7 and 2.5 GeV/c. A partial-wave analysis of the data has verified the $J^P=\frac{7}{2}^+$ assignment for the $\Delta(1950)$ and established the $N(2190)$ as $J^P=\frac{7}{2}^-$. Other structures in the partial-wave amplitudes could be interpreted as highly inelastic resonances, but the ambiguities inherent in a many-parameter phase-shift analysis prevent us from making any claims.

In the energy region analyzed, we observe the bulk of the transition from the resonance region to the high-energy region where the partial-wave amplitudes are correlated and change slowly with energy. We observe that at the higher energies of the analysis the imaginary parts of the partial-wave amplitudes exhibit a systematic dependence upon the angular momentum l, but that this dependence is different for $J=l+\frac{1}{2}$ and $J=l-\frac{1}{2}$. Also, in the amplitudes A' and B, which are usually used to represent high-energy scattering, we see the onset of structure which becomes stationary in t as the energy is increased and which appears to be associated with the structure that appears in cross sections and polarizations at much higher energies.

ACKNOWLEDGMENTS

We wish to acknowledge the cooperation and support of Dr. T. H. Fields, Dr. L. C. Teng, and the staff of the Argonne zero-gradient synchrotron. Special thanks are due to A. Moretti for his tireless efforts in the development and operation of the polarized target, and to J. Simanton for the design of much of the electronic logic system. We are grateful to Professor C. D. Jeffries for his help and guidance in the construction of this polarized proton target. Our thanks go to R. Marquardt, K. Bourkland, and D. Amundson for construction of the target electronics, to Marie Gawlik for growing the target crystals, to R. George for some programming help, and to J. Scheid for assistance during the experiment.

---

[48] K. S. Heard, Ph.D. thesis, University of Oxford, 1967 (unpublished).

[49] C. R. Cox, P. J. Duke, K. S. Heard, R. E. Hill, W. R. Holley, D. P. Jones, F. C. Shoemaker, J. J. Thresher, J. B. Warren, and J. C. Sleeman, Phys. Rev. **184**, 1453 (1969).

[50] P. S. Alpin, I. M. Cowan, W. M. Gibson, R. S. Gilmore, K. Green, J. Malos, V. J. Smith, D. L. Ward, M. A. R. Kemp, and R. McKenzie, Rutherford Laboratory Report No. RPP/H/44, 1969 (unpublished).